

# Institutionen för systemteknik

## Department of Electrical Engineering

Examensarbete

### Virtual Sensors for Combustion Parameters Based on In-Cylinder Pressure

Master's thesis performed in Vehicular Systems  
at Linköping University  
by

**Tobias Johansson**

LiTH-ISY-EX--15/4913--SE

Linköping 2015



**Linköpings universitet**  
**TEKNISKA HÖGSKOLAN**



# Virtual Sensors for Combustion Parameters Based on In-Cylinder Pressure

Master's thesis performed in Vehicular Systems  
at Linköping University  
by

**Tobias Johansson**

LiTH-ISY-EX--15/4913--SE

Supervisor: **Dr. Andreas Thomasson**  
ISY, Linköping University  
**Dr. Ola Stenlås**  
Scania AB

Examiner: **Professor Lars Eriksson**  
ISY, Linköping University

Linköping, June 18, 2015



	<b>Avdelning, Institution</b> Division, Department	<b>Datum</b> Date
	Division of Vehicular Systems Department of Electrical Engineering SE-581 83 Linköping	2015-06-18

<b>Språk</b> Language <input type="checkbox"/> Svenska/Swedish <input checked="" type="checkbox"/> Engelska/English <input type="checkbox"/> _____	<b>Rapporttyp</b> Report category <input type="checkbox"/> Licentiatavhandling <input checked="" type="checkbox"/> Examensarbete <input type="checkbox"/> C-uppsats <input type="checkbox"/> D-uppsats <input type="checkbox"/> Övrig rapport <input type="checkbox"/> _____	<b>ISBN</b> _____ <b>ISRN</b> LiTH-ISY-EX--15/4913--SE <b>Serietitel och serienummer</b> <b>ISSN</b> Title of series, numbering                      _____
--	---	---

**URL för elektronisk version**

<http://urn.kb.se/resolve?urn=urn:nbn:se:liu:diva-XXXXX>

<b>Titel</b> Title	Skattning av förbränningsparametrar baserat på cylindertryckmätning Virtual Sensors for Combustion Parameters Based on In-Cylinder Pressure
<b>Författare</b> Author	Tobias Johansson

**Sammanfattning**  
 Abstract

Typically the combustion in engines are open-loop controlled. By using an in-cylinder pressure sensor it is possible to create virtual sensors for closed-loop combustion control (CLCC). With CLCC it is possible to counteract dynamic effects as component ageing, fuel type and cylinder variance.

A virtual sensor system was implemented based on a one-zone heat-release analysis, including signal processing of the pressure sensor input. A parametrisation of the heat-release based on several Vibe functions was implemented with good results.

The major focus of the virtual sensor system was to perform a tolerance analysis on experimental data, where typical error sources in a production heavy-duty vehicle were identified and their effect on the estimates quantified. It could be concluded that estimates are very much dependent on the choice of heat-release and specific heat ratio models. Especially crank angle phasing has a large impact on estimation performance, stressing the importance of accounting for crankshaft torsion in production vehicles. Biodiesel advances the combustion angle and give a lower IMEP and total heat amount compared to standard diesel. However, error sensitivity is not affected.

Further investigations must be made on improving the signal processing in terms of gain error compensation and filtering. Also a better understanding of how errors propagate between subsystems in a CLCC system is required for successful implementation.

<b>Nyckelord</b> Keywords	CLCC, Virtual sensors, combustion parameters, in-cylinder pressure
------------------------------	--



## **Abstract**

Typically the combustion in engines are open-loop controlled. By using an in-cylinder pressure sensor it is possible to create virtual sensors for closed-loop combustion control (CLCC). With CLCC it is possible to counteract dynamic effects as component ageing, fuel type and cylinder variance.

A virtual sensor system was implemented based on a one-zone heat-release analysis, including signal processing of the pressure sensor input. A parametrisation of the heat-release based on several Vibe functions was implemented with good results.

The major focus of the virtual sensor system was to perform a tolerance analysis on experimental data, where typical error sources in a production heavy-duty vehicle were identified and their effect on the estimates quantified. It could be concluded that estimates are very much dependent on the choice of heat-release and specific heat ratio models. Especially crank angle phasing has a large impact on estimation performance, stressing the importance of accounting for crankshaft torsion in production vehicles. Biodiesel advances the combustion angle and give a lower IMEP and total heat amount compared to standard diesel. However, error sensitivity is not affected.

Further investigations must be made on improving the signal processing in terms of gain error compensation and filtering. Also a better understanding of how errors propagate between subsystems in a CLCC system is required for successful implementation.



## Acknowledgements

There are so many people I would like to thank, all of whom have helped me to get where I am today.

First of all, I would like to thank Scania for giving me the opportunity to write this thesis. The knowledge and experience I have acquired during these past few months have affected me both personally and professionally. I sincerely hope that Scania will continue to collaborate with universities to give future students the possibilities I have been given.

I would like to thank my supervisors Ola Stenlåås and Andreas Thomasson, without their support and constructive comments I would never have been able to finish this thesis. Also I would like to thank Stephan Zentner who always kindly offered me his time to discuss various topics about heat-release, Porsche and everything in-between.

A thank you to Vehicular Systems at Linköping University, who together with ISY have the best and most engaging courses at the university! I hope you will continue in the same spirit and keep developing your courses. A thank you to my examiner Lars Eriksson, who is partly responsible that I chose control engineering as my Master's degree.

A warm thank you to my fellow thesis workers at NESC, who like me had the opportunity to finish their educations at Scania. You have given me a lot of laughs and engaging discussions at "fika" breaks, but also been there to help me when needed.

My dear friends and classmates, Erik, Petter and Oskar, who have become my second family in Linköping. I am so grateful to have met you and to have been given three lifelong friendships. We have experienced so much together and I look forward to all the fun we will have in the future!

Finally, I would like to thank my family who has always been there for me no matter what. Your support is a big reason why I have managed to keep on going during these past five years. From now on I will hopefully be able to see you a lot more again.

A big thank you to everyone involved!

*Södertälje, June 2015  
Tobias Johansson*



---

# Contents

<b>Notation</b>	<b>ix</b>
<b>1 Introduction</b>	<b>1</b>
1.1 Objectives . . . . .	2
1.2 Delimitations . . . . .	2
1.3 Related work . . . . .	3
1.4 Outline . . . . .	4
<b>2 Theory</b>	<b>7</b>
2.1 The combustion cycle of the four-stroke CI-engine . . . . .	7
2.1.1 The four-stroke cycle . . . . .	7
2.1.2 Combustion development during fuel injection . . . . .	8
2.2 Heat-release analysis . . . . .	9
2.2.1 Definitions of the relevant combustion parameters . . . . .	10
2.3 Pressure transducers . . . . .	13
2.3.1 The piezoelectric transducer . . . . .	13
2.3.2 The piezoresistive transducer . . . . .	14
2.3.3 The optical transducer . . . . .	14
2.3.4 Absolute pressure referencing . . . . .	14
2.4 Signal processing . . . . .	15
2.4.1 Filters . . . . .	15
2.4.2 Sampling . . . . .	16
2.4.3 Aliasing . . . . .	17
<b>3 Data acquisition</b>	<b>19</b>
3.1 Experimental set-up . . . . .	19
3.2 Data sampling . . . . .	21
3.3 Experimental procedure . . . . .	22
<b>4 Modelling</b>	<b>25</b>
4.1 Signal processing of pressure sensor signal . . . . .	25
4.1.1 Constant filter techniques . . . . .	26
4.1.2 Filter with adaptive cutoff frequency . . . . .	26

4.1.3	Cylinder pressure sensor model . . . . .	28
4.1.4	Compensation for zero-level drift . . . . .	28
4.1.5	Estimating TDC position . . . . .	29
4.2	Heat-release model . . . . .	31
4.2.1	Calculation of pressure derivative, volume and area . . . . .	32
4.2.2	Specific heat ratio . . . . .	32
4.2.3	Algorithm . . . . .	33
4.3	Heat-release parametrisation by Vibe functions . . . . .	35
4.4	Virtual sensors for the combustion parameters . . . . .	36
4.4.1	Maximum pressure . . . . .	36
4.4.2	Compression ratio estimation . . . . .	36
4.4.3	SOC and ignition delay . . . . .	37
4.4.4	IMEP and indicated torque . . . . .	38
4.4.5	CAX and combustion duration . . . . .	38
4.4.6	Engine efficiency . . . . .	39
4.4.7	Heating value of fuel . . . . .	39
<b>5</b>	<b>Results</b>	<b>41</b>
5.1	Filtering . . . . .	42
5.2	Cycle-to-cycle variations . . . . .	42
5.3	Absolute pressure referencing . . . . .	42
5.4	Pressure sensor gain error . . . . .	45
5.5	Specific heat ratio . . . . .	46
5.6	Heat-release models . . . . .	47
5.6.1	Woschni heat transfer parameters . . . . .	48
5.7	Crank angle phasing . . . . .	49
5.8	Compression ratio . . . . .	50
5.9	Intake manifold sensor errors . . . . .	51
5.10	Trapped mass error . . . . .	51
5.11	Effect of fuel type . . . . .	52
5.12	Validation of parametrisation model . . . . .	52
<b>6</b>	<b>Conclusions</b>	<b>55</b>
	<b>Bibliography</b>	<b>57</b>



# Notation

Variable	Description
$A$	Cylinder wall area
$Q$	Cumulative heat-release
$R$	Crank ratio, or ideal gas constant depending on context
$T$	Cylinder charge temperature
$T_{gas}$	Gas (or indicated) torque
$V$	Instantaneous cylinder volume
$V_d$	Cylinder displacement volume
$a$	Design parameter in the Wiebe function
$c_p$	Specific heat at constant pressure
$c_v$	Specific heat at constant volume
$m$	Design parameter in the Wiebe function
$m_f$	Injected fuel mass
$p$	Cylinder pressure
$q_{LHV}$	Lower heating value of the fuel
$r_c$	Compression ratio
$x_b$	Mass fraction burned from Wiebe function parametrization
$\beta$	Design parameter in the Wiebe function
$\gamma$	Specific heat ratio
$\eta$	Efficiency
$\theta$	Crank angle
$\theta_{CAx}$	Crank angle at X % fuel burnt
$\theta_{SOC}$	Crank angle at SOC
$\theta_{SOI}$	Crank angle at SOI
$\theta_d$	Combustion duration in crank angles
$\theta_{ign}$	Crank angle at ignition (SOC)
$\theta_{res}$	Sampling resolution in CAD
$\kappa$	Polytropic index
$\lambda$	Relative air/fuel ratio
$\tau$	Ignition delay
$\frac{dQ}{d\theta}$	Heat-release rate
$\frac{dQ_{ht}}{d\theta}$	Heat transfer rate
$\frac{dV}{d\theta}$	Cylinder volume derivative with respect to CA
$\frac{dp}{d\theta}$	Cylinder pressure derivative with respect to CA

---

<b>Abbreviation</b>	<b>Description</b>
ASI	After Start of Injection
ATDC	After Top Dead Centre
BDC	Bottom Dead Centre
CA	Crank Angle
CAD	Crank Angle Degree
CAX	Crank angle at X % fuel burnt
CLCC	Closed-Loop Combustion Control
CI	Compression Ignition
DFT	Discrete Fourier Transform
ECU	Engine Control Unit
EOC	End Of Combustion
HDV	Heavy-Duty Vehicle
HR	Heat-Release
HRR	Heat-Release Rate
HCCI	Homogeneous Charge Compression Ignition
IBDC	Intake Bottom Dead Centre
ICE	Internal Combustion Engine
IMEP	Indicated Mean Effective Pressure
MFB	Mass Fraction Burned
RME	Rapeseed Methyl Ester
MAP	Intake Manifold Pressure
SOC	Start Of Combustion
SOI	Start Of Injection
TDC	Top Dead Centre
VVT	Variable Valve Timing

---



# 1

---

## Introduction

With the ever stringent emissions legislature and requirement of higher fuel efficiency, the complexity of the internal combustion engine (ICE) is increasing. The advent of new engine types like the homogeneous charge compression ignition (HCCI) requires even more advanced engine control compared to ordinary compression ignition (CI) engines.

The engine control of today is mainly based on open-loop using engine maps with large sets of operating points. After the introduction of the Euro 6 emission standards, the required emission management have considerably increased the number of operating modes of the engine. The development cost grows rapidly due to the added calibration time and complexity of the modes and maps. The incentives of moving towards closed-loop combustion control (CLCC) in production vehicles are therefore increasing.

To realise CLCC quantitative measures of the combustion process in the cylinder are required. What parameters to use and the accuracy of those are of vital importance when developing the CLCC systems. Historically the analysis of cylinder pressure has been the primary way to quantify the combustion process because of the thermodynamic relationship to the combustion. However, issues related to cost, reliability and life expectancy prohibited the use of in-cylinder pressure sensors in production vehicles. Instead several methods of estimating the pressure trace have been developed. Advancements in sensor technology have made the sensor approach possible, at least in lightweight vehicles [1, 2]. If the sensor durability is further enhanced and the cost is decreased, it may be a viable option in the heavy-duty vehicle (HDV) industry. Scania AB acknowledges the possibilities of the technology advance and wants to investigate the choice of using in-cylinder pressure measurements compared to reconstructed pressure traces,

and how it affects the combustion parameter estimations.

## 1.1 Objectives

The main goal for this thesis is to, based on in-cylinder pressure, create combustion parameter estimators to be used in CLCC of a heavy-duty CI-engine. More specifically the

- mass fraction burned estimates CA10, CA50, CA90 (crank angle at X % fuel mass burned),
- maximum cylinder pressure  $p_{max}$ ,
- top dead centre (TDC) position,
- amount of fuel injected  $m_f$ ,
- engine efficiency,
- compression ratio,
- ignition delay  $\tau$ ,
- indicated (gas) torque.

The estimation models will be based on thermodynamic relationships or calculated directly from pressure measurements. A tolerance analysis of the estimated combustion parameters must be performed to assess if and under what circumstances the parameters are accurate enough for CLCC. Another objective is to investigate how to dynamically adjust the combustion behaviour to offset factors as fuel quality, engine geometry variations and ageing. The complexity of the algorithms should be balanced between computation effort and accuracy since the goal is to implement them in a future real-time control system.

Three other theses are being carried out in close proximity, with some common areas that will be collaborated on. These are high-resolution crank angle degree (CAD) estimation and in-cylinder pressure estimation. Accurate CAD computation is of vital importance to the viability of the model-based control approach. An investigation will be made on the possible improvements of the estimations of CAD and combustion parameters by sharing data in both directions. Additionally, the effect on the combustion parameter accuracy by using an estimated pressure trace based on both a knock sensor and CAD will be analysed.

## 1.2 Delimitations

The scope of the thesis is confined within the following delimitations:

- The fuel injector geometry and positioning will not be analysed.
- The possibilities of adjusting the fuel injection strategy will not be considered.

- No analysis will be made on the formation of emissions.
- The design and control of the gas exchange will not be evaluated.
- Experimental data will only be collected from an inline six-cylinder Scania engine.
- Multi-zone heat-release models will not be treated.
- The parameter calculations and tolerance analysis will be restricted to Matlab/Simulink. No finished production code will be delivered.
- Since the thesis is looking at future possibilities of CLCC, the hardware limitations of the present ECU will not be considered. The future ECU is assumed to have upgraded hardware to support the increased computations required in the model-based control.
- Diagnostic capabilities are not treated. How the virtual sensors can be implemented in a diagnostic system is subject to future work.
- A combustion control system will not be developed, e.g. using the developed virtual sensors to control the injection timing.
- It is assumed that calculations will be performed on complete pressure cycles, thereby having all samples available at the time of calculations.

### 1.3 Related work

Research on CLCC has sparked during the last ten to fifteen years. There are several publications discussing topics related to it. In-cylinder pressure and its importance to the engine combustion analysis is summarised in [3]. There are numerous proposed methods on how to quantify the combustion process by pressure traces. The most widespread method for CI engines is the use of heat-release analysis. Single-zone heat-release models based on the thermodynamic first law are the commonly proposed method [4, 5]. However, the analysis is in no way an easy task due to the complexity of the combustion. The problems are connected to the inaccuracies of the heat-release model and measurement errors. The specific heat ratio  $\gamma$ , charge to wall heat transfer and pressure measurements errors are considered as the main areas of inaccuracy [6].

The authors of [7] highlights another weakness of the one-zone heat-release, the homogeneous charge assumption, and its effect on initial and final values of the heat-release rate. The rate is underestimated initially and overestimated in the final part of the combustion. However, the total cumulative heat-release for a complete cycle is accurate. The inaccuracies of the single-zone heat-release model is apparently higher at low load and low burn rates [8].

A more thorough investigation of the specific heat ratio and an evaluation of a proposed model is presented in [9]. In [10] the accuracy of the heat-release analysis

using single-zone first law models is investigated and quantified. Two alternative models are proposed which show good results and acceptable accuracy.

One of the most common approaches to model the heat transfer is the relation created by Woschni [11]. At its core it is a convective heat transfer model based on a Nusselt-Reynolds number relation.

To increase the accuracy of the analysis there have been extensive research about the phenomenons affecting the pressure transducer and its measurements. The main causes of inaccuracies is connected to absolute pressure referencing methods (i.e. pegging), crank angle phasing, signal drift and different kinds of noise (mechanical, electrical) [12, 13]. The choice of transducer will affect what errors are emphasized in the signal processing due to the different characteristics of the available transducers.

The common method of crank angle phasing is the determination of the TDC position. It can be done in several ways; thermodynamic relationships [14, 15], using the symmetry of the cylinder pressure in a motored cycle [16], or the use of a TDC sensor [17].

There are several pegging methods based on referencing external sensors or by assuming a polytropic process and use different types of curve-fitting [18, 19]. It seems as referencing the transducer output at inlet bottom dead center (IBDC) to the intake manifold pressure (MAP) gives the highest accuracy given low speeds. At high speeds the approach is prone to errors due to tuned intake runners and pressure drop over the intake valve.

In production vehicles the computation capacity is generally restricted. This is an issue when deploying heat-release analysis and model-based control which is considerably more computation expensive than engine maps and open-loops. Real-time implementations are demonstrated together with a new algorithm based on pressure ratio in [20]. The paper also treats the effects of the specific heat ratio temperature dependence and charge-to-wall heat transfer. There is another paper evaluating the pressure ratio by the same authors, where it is confirmed that the algorithm is suitable in real-time applications for calculation of CA50 [21].

As a response to the historical issues, cost and durability, related to in-cylinder pressure sensors and production vehicles, there are numerous approaches of calculating combustion parameters by estimating the in-cylinder pressure instead of using measurements. The virtual sensors are based on e.g. speed sensors [22], accelerometers [23] and ion-sensing [24, 25]. Another common approach is to use Vibe functions as a mean to parametrise and model the heat-release [26].

## 1.4 Outline

The first chapter introduces the background and problem statement of the thesis with a short walk-through of previous work in the area. Important theory necessary to understand the content is presented in chapter two. It introduces the

---

four-stroke engine, heat-release analysis, combustion parameter definitions and signal processing. The third chapter describes the data acquisition, e.g. the equipment used and acquisition methodology. The fourth chapter describes the models and algorithms implemented to achieve the results that this thesis is based upon. The results are presented in chapter five with a thorough discussion of important findings. Finally, chapter six contains the conclusions based on the results chapter and also presents suggestions of future work.



# 2

---

## Theory

### 2.1 The combustion cycle of the four-stroke CI-engine

In this section conceptual explanations are provided for the four-stroke cycle and the combustion development during fuel injection in a CI-engine.

#### 2.1.1 The four-stroke cycle

A four-stroke cycle comprise of the intake, compression, power (or expansion), and exhaust strokes. For a CI-engine, the working principle is:

1. Intake: The intake valve is open and fresh air fills the cylinder as the piston moves from TDC to BDC.
2. Compression: The trapped air charge is compressed when the piston moves towards TDC, with an increase in pressure and temperature. At the end of the compression stroke, just before TDC, fuel is injected and the combustion is initiated when the fuel begins to ignite.
3. Power: At TDC, the power stroke starts and the hot, high-pressure gases force the piston towards BDC. Around 140 degrees ATDC, the exhaust valve opens and exhaust gas begins to flush out of the cylinder in a blow-down process.
4. Exhaust: The remaining combustion gases are ventilated as the piston moves toward TDC again.

The intake valve can close before or after BDC when going from intake to compression stroke, depending on wanted engine performance. Some engines also

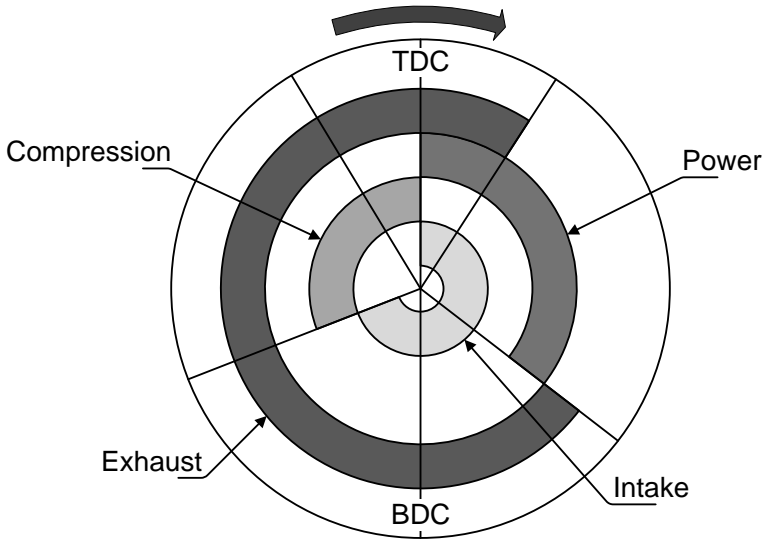


**Figure 2.1:** A conceptual figure of how the strokes in a four-stroke cycle is divided. The cycle begins at the inner arc and progress outwards, with the exhaust stroke being the outer arc. Every transition has a valve opening or closing. Note that this is only one example of a cycle, the exact valve timings are different between engines and can change depending on operating point if VVT is in use.

use valve overlap between exhaust and intake strokes, i.e. the intake valve is opened before TDC while the exhaust valve closes after TDC, to improve the filling of fresh air. Today, it is common to adjust the valve timings depending on operating point with a variable valve timing (VVT) system. It assists in improving performance, fuel economy and emissions over the complete engine operating range compared to fixed valve timings.

### 2.1.2 Combustion development during fuel injection

The combustion process during the power stroke is very complex and still not fully understood. The classical approach described by Heywood [5] consists of three main parts; ignition delay, premixed combustion and mixing-controlled combustion. The different parts can be deduced from the HRR diagram derived from the pressure data. Research by John Dec has enlightened how the fuel spray and flame develops in each of these three parts. For an exhaustive explanation of the combustion process together with a graphical description, see John Dec paper [27], and more specifically Figure 17.

Ignition delay is the time between start of injection (SOI) of fuel and the actual start of combustion (SOC). The delay is caused by atomisation of fuel, heating, vapourisation, mixing of air and fuel and chemical pre-combustion reactions. When

liquid fuel is injected it begins to vaporise when heated by the surrounding hot air. The region closest to the injector contains only liquid fuel, and gradually the presence of vaporised fuel increases downstream. A vapour-fuel region develops along the sides of the fuel jet at 2° ASI and grows thicker until the liquid fuel jet reaches its maximum penetration at 3° ASI. Gases mix with air along the periphery of the fuel spray and in the head-vortex, forming a rich mixture of  $\lambda = 0.25-0.5$ . This relatively uniform mixture auto-ignites in the range 3° – 5° ASI at multiple points in the downstream jet.

Premixed combustion is the first phase of combustion where heat is released very rapidly from the rich vapour-fuel/air mixture. This can be identified as the start of the rapid increase in the heat-release rate (HRR) curve (see section 2.2). The fuel starts to break down at 5° ASI and PAHs<sup>1</sup> form in the rich mixture section.

As the combustion continues, soot occurs throughout the downstream portion of the jet at 6.5° ASI. Parallel to soot formation a diffusion flame develops at the periphery of the downstream jet. The fuel jet continues to penetrate the combustion chamber with an increasing concentration of soot in the head-vortex region which can be seen at 8° ASI. From this point, the combustion transitions to mixing-controlled as the last fractions of premixed air are consumed. In the mixing-controlled phase the combustion is mainly controlled by the vapour-fuel/air mixing process. In the HRR curve in Figure 2.2, the mixing-controlled phase occurs after the maximum peak.

## 2.2 Heat-release analysis

When the combustion is finished the fuel has converted into gaseous emissions by hundreds of chemical reactions. As a by-product a tremendous amount of heat is released, which causes the pressure to increase in the combustion chamber. Due to the direct correlation between pressure and heat it is possible to analyse the complex combustion process by exploiting the knowledge on cylinder pressure.

Common practice is to deploy a heat-release analysis based on the first law of thermodynamics and the ideal gas law. Usually a one-zone description is developed, i.e. the contents of the cylinder are considered homogeneous. By assuming an ideal gas and constant  $R$  (i.e. the amount of moles and the specific heats are constant), the *gross* heat-release can be written as

$$\frac{dQ_{gross}}{d\theta} = \frac{\gamma}{\gamma-1} p \frac{dV}{d\theta} + \frac{1}{\gamma-1} V \frac{dp}{d\theta} + \frac{dQ_{ht}}{d\theta} + \frac{dQ_{crevice}}{d\theta} \quad (2.1)$$

where  $\gamma = c_p/c_v$  is the specific heat ratio,  $p$  cylinder pressure,  $V$  cylinder volume,  $Q_{ht}$  heat transfer losses and  $Q_{crevice}$  crevice flow losses. The specific heat ratio is difficult to determine accurately. Depending on required accuracy it is either set constant or modelled as a function of temperature.

<sup>1</sup>Polycyclic Aromatic Hydrocarbons, produced from incomplete combustion caused by a lack of oxygen.

Since the inaccuracies of the losses are considered high and they requires extra computing power, the *net* heat-release is often used in practice, i.e. the losses are neglected. The equation then describes the rate at which work is done on the piston and the rate of change of internal energy. With this simplification Eq. (2.1) can be written as [5]

$$\frac{dQ_{net}}{d\theta} = \frac{\gamma}{\gamma - 1} p \frac{dV}{d\theta} + \frac{1}{\gamma - 1} V \frac{dp}{d\theta} \quad (2.2)$$

By knowing the pressure and volume at a given crank angle or time the HRR can be calculated. The accuracy of this calculation is very dependent on the quality of the inputs, especially the pressure. Additional problems arise due to the dependency of derivatives in the calculation. To achieve satisfactory results, extensive measures must be taken to process the signal inputs.

The HRR can be integrated to get the cumulative heat released in the combustion,

$$Q = \int_{\theta_{start}}^{\theta_{end}} \frac{dQ}{d\theta} d\theta \quad (2.3)$$

where  $\theta_{start}$  and  $\theta_{end}$  are the angles where start and end of combustion occurs.

By examining the cumulative heat-release extensive information about combustion duration, crank angle at a specific fuel percentage burnt etc. can be found.

### 2.2.1 Definitions of the relevant combustion parameters

There are a lot of parameters available to quantify the combustion process. The most relevant will be presented and defined in this section.

**Maximum cylinder pressure**  $p_{max}$  is an important design parameter that is restricted by the hardware limitations of the engine. Calibrating the engine to work close to specified maximum usually correlates with a higher thermal efficiency while it is important to stay below maximum to avoid engine failure. Maximum pressure is easy to calculate given a cylinder pressure sensor,

$$p_{max} = \max(p_{cyl}(\theta)) \quad (2.4)$$

and the corresponding angle

$$\theta_{p_{max}} = \arg \max_{\theta} (p_{cyl}(\theta)) \quad (2.5)$$

**SOC** Acronym for start of combustion. Defines the point where combustion is initiated. The position of the SOC has a strong impact on the combustion behaviour, which in turn affects the engine work and efficiency. Early SOC gives a higher pressure build-up and larger peaks with lower pressure during later parts of the expansion stroke compared to late SOC position. Too early SOC and

pressure build-up counteracts the compression stroke, increasing the losses. Too late SOC and the work is decreased due to not fully using the expansion stroke. There is an optimal point where the losses are at a minimum, resulting in the highest engine efficiency. This point is of course the goal when calibrating the engine. With open-loop control however, there is no way of assuring optimal SOC position during the complete engine lifespan [28]. The actual SOC position can be found visually by identifying the point where the HRR curve start to rapidly increase, but no heat has yet been released. Mathematically it can be defined as

$$\begin{aligned} Q(\theta_{SOC}) &= 0 \\ \frac{dQ(\theta_{SOC})}{d\theta} &> 0 \end{aligned} \quad (2.6)$$

**CAx** The crank angle definitions that will be used in this paper are crank angle at 10 %, 50 % and 90 % fuel burnt ( $\theta_{CA10}$ ,  $\theta_{CA50}$ ,  $\theta_{CA90}$  respectively), see Figure 2.2.

$\theta_{CA10}$  is often used as an indication of SOC, due to the inaccuracies and noise close to 0. It is defined by

$$Q(\theta_{CA10}) = 0.1 \cdot \max(Q) \quad (2.7)$$

$\theta_{CA50}$  defines the point where the bulk of combustion occurs and is often used as a mean to quantify the position of combustion. It is defined by

$$\theta_{CA50} = \arg \max_{\theta} \left( \frac{dQ(\theta)}{d\theta} \right) \quad (2.8)$$

or

$$Q(\theta_{CA50}) = 0.5 \cdot \max(Q) \quad (2.9)$$

Finally,  $\theta_{CA100}$  defines the end of combustion. It is often replaced by  $\theta_{CA90}$  due to the numerical issues close to the combustion boundaries when the rate of heat released is very small. It is defined by

$$Q(\theta_{CA90}) = 0.9 \cdot \max(Q) \quad (2.10)$$

**Combustion duration** The combustion duration is defined as the angle or time difference between 0% and 100% fuel burnt. Often expressed as the angular distance between  $\theta_{CA10}$  and  $\theta_{CA90}$ . It is defined by

$$\theta_d = \theta_{CA90} - \theta_{CA10} \quad (2.11)$$

**IMEP** Another common parameter is the indicated mean effective pressure (IMEP). It is basically engine work normalised with the cylinder displacement volume,

$$IMEP = \frac{W_i}{V_d} = \frac{1}{V_d} \oint p dV \quad (2.12)$$

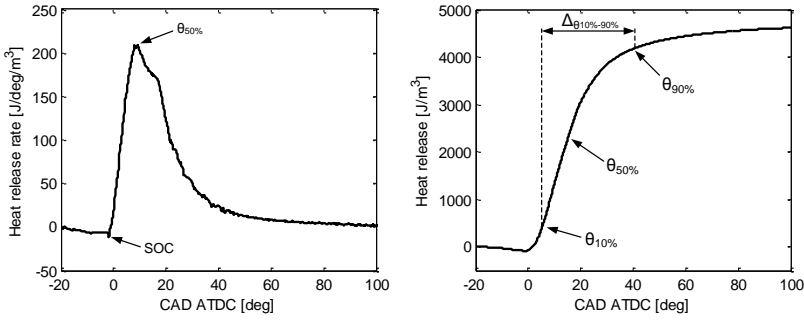


**Figure 2.2:** Heat-release rate and cumulative heat-release rate diagrams with the  $\theta_x$  specified. The data has been normalised with the cylinder displacement volume.

where  $W_i$  is the indicated work and  $V_d$  is cylinder displacement volume. By choosing whether the work is integrated over the whole four-stroke cycle or only the compression and expansion strokes, the *net* IMEP or *gross* IMEP is calculated. IMEP can be seen as the constant pressure required to accomplish the same amount of work as the real working cycle.

**Indicated torque** Given a pressure trace of every cylinder, the instantaneous indicated torque of the engine can be described by

$$T_{gas}(\theta) = \sum_{j=1}^{n_{cyl}} (p_{cyl,j}(\theta - \theta_j^0) - p_{amb})AL(\theta - \theta_j^0) \quad (2.13)$$

where  $p_{cyl,j}$  is the pressure trace of cylinder  $j$ ,  $\theta_j^0$  is the cylinder individual offset,  $A$  is the piston area,  $L$  is the crank lever. The product  $AL(\theta)$  is equal to the volume derivative  $\frac{dV}{d\theta}$  [28]. Note that  $T$  is torque in this equation and not temperature.

**Compression ratio** The compression ratio,  $r_c$ , is the ratio between maximum and minimum cylinder volume. The minimum volume is  $V_c$ , and the maximum volume is the sum of displaced volume,  $V_d$ , and  $V_c$ . It is defined as

$$r_c = \frac{V_d + V_c}{V_c} \quad (2.14)$$

**TDC position** Calibration of the crank angle is of vital importance when performing heat-release analysis. A cylinder pressure trace that is measured with a crank angle phasing error larger than  $0.1^\circ$  can give considerable deviations in peak HRR and cumulative HRR. Due to mechanical tolerances and torsion in the crankshaft it is impossible to mount the crank angle sensor without some offset.

Determining the TDC position is usually done by motored cycles with no fuel injection. Typically only the constant offset is corrected while the component from torsion is very difficult to compensate since it varies within a cycle but also with load and speed. A method presented by Tunestål [29] to compensate for constant phasing offset showed good results with low noise sensitivity which is based on the net heat-release model. See section 4.1.5 for a thorough description of the methodology.

**Mass of fuel injected** The amount of fuel injected  $m_f$  can be written as

$$m_f = \frac{Q_{in}}{\eta_f \cdot q_{LHV}} \quad (2.15)$$

where  $Q_{in}$  is the total amount of energy released,  $\eta_f$  is the combustion efficiency and  $q_{LHV}$  is the lower heating value of the fuel. A rough estimation is achieved by using the maximum of the cumulative HRR,  $\max(Q_{net})$ . An alternative approach may be used where Eq. 2.15 is rewritten by using  $\lambda$ , stoichiometric air/fuel ratio  $\left(\frac{A}{F}\right)_s$  and residual gas fraction  $x_r$  [30]

$$m_f = \frac{(1 - x_r)m_{tot}}{\lambda \left(\frac{A}{F}\right)_s} \quad (2.16)$$

If EGR is present the model can be expanded by estimating the fraction of EGR,  $x_{EGR}$ , in the fresh air charge. Note that Eq. (2.16) is only valid in steady-state.

**Engine efficiency** The total efficiency is the complete chain of conversion from chemical energy stored in the injected fuel to the actual work output of the engine. It consists of several parts as mechanical efficiency, gas exchange efficiency, thermal efficiency and combustion efficiency. It can be written as [28]

$$\eta = \frac{W}{q_{LHV} \cdot m_f} = \frac{\dot{W}}{q_{LHV} \cdot \dot{m}_f} \quad (2.17)$$

where  $W$  is the work output of the engine.

## 2.3 Pressure transducers

Cylinder pressure measurements can be performed by using several kinds of transducers types. The most common types in use are the piezoelectric, piezoresistive and optical transducers. The choice of transducer will depend on desired bandwidth, measuring accuracy (drift, robustness) and cost.

### 2.3.1 The piezoelectric transducer

This transducer type makes use of the piezoelectric effect, which was first discovered by Pierre and Jacques Curie in 1880. The discovery was that a quartz crystal

becomes electrically charged when there is a change in the external forces acting on it [31].

The electrical charge is converted by a charge amplifier which converts it to either a voltage or a current. The output indicates the change in pressure. Due to the fundamental principle of the piezoelectric transducer, it can only measure the relative pressure and not the absolute pressure. This requires the sensor signal to be referenced to a zero-level to be a useful measurement. This can be done by referencing to another sensor, e.g. the absolute pressure sensor in the inlet manifold, or by using knowledge about the polytropic process [18, 19].

### 2.3.2 The piezoresistive transducer

The piezoresistive transducer changes its electrical resistivity when being subject to mechanical strain caused by an external force. A fundamental weakness of the piezoresistive transducers is the relatively small temperature range. It also suffers from temperature-dependent characteristics, e.g. zero-line shift, change of linearity and varying sensitivity [32].

The cylinder pressure transducer in use by Volkswagen in their production vehicles is of this type [2, 33].

### 2.3.3 The optical transducer

An optical transducer is principally consisting of; a sensing head with a metal diaphragm exposed to the combustion pressure, a LED, a photo-diode and fiber-optic cables. The LED emits light which is reflected on the sensing head diaphragm and received by the photo-diode, which measures the intensity of the reflected light. The benefits of this transducer is its low cost and durability [34].

### 2.3.4 Absolute pressure referencing

When using a transducer with relative pressure indication the output must be referenced to the absolute pressure somewhere in the cycle. This is commonly referred to as "pegging". This can be done every cycle or once for each series of cycles. By pegging every cycle the long-term drift is minimized [19].

There are several pegging methods available. A common way is to set the cylinder pressure equal to the inlet manifold pressure (MAP) at a point in the cycle, usually around intake bottom dead center (IBDC). This method is very accurate at low speeds. However, choosing a good crank angle point is difficult due to the pressure wave formation in the intake runners. To decrease the effect of noisy MAP measurements an average pressure over several points around IBDC can be used as the pegging value.

Another common way is to utilize the knowledge about polytropic processes. By assuming the compression after IVC to be a reversible adiabatic (isentropic) process, i.e. no heat exchange with the surroundings, it follows

$$pV^{\kappa} = C \quad (2.18)$$

where  $n = \kappa$  for an isentropic process and  $C$  is a constant. By assuming the measured voltage,  $E$ , can be written as a function of sensor gain,  $K_s$ , and constant bias,  $E_{bias}$ , as

$$E(\theta) = K_s \cdot p(\theta) + E_{bias} \quad (2.19)$$

the sensor offset can be calculated together with Eq. (2.18). By using two-point referencing with a fixed  $\kappa$  the bias can be written as

$$E_{bias} = \frac{E(\theta_1) - E(\theta_2)[V(\theta_2)/V(\theta_1)]^\kappa}{1 - [V(\theta_2)/V(\theta_1)]^\kappa} \quad (2.20)$$

which gives an estimate of the bias in the pressure signal.

## 2.4 Signal processing

It is a well-known problem that differentiation amplifies the noise in the data. Since the differentiated pressure  $\frac{dp}{d\theta}$  is required when calculating the HRR in Eq. (2.2), the noise in the pressure data must be reduced. This is also true when using data that is averaged over several cycles. The averaging improves the signal-to-noise ratio, though it is not enough to eliminate the problem. Three approaches to overcome the issue of noisy data are:

1. Low-pass filter the pressure data when differentiating.
2. Construct a function using curve fitting that captures the behaviour of the pressure data, and differentiate the function.
3. Avoid the use of  $\frac{dp}{d\theta}$  by integrating Eq. (2.2) and analytically evaluate the integral containing the pressure derivative [31].

What path to choose is a matter of data quality, computation requirements, online or offline application etc.

### 2.4.1 Filters

Filters are generally categorised as *finite impulse response* (FIR) or *infinite impulse response* (IIR) filters [35]. As the name suggests the former has a finite impulse while the latter has an infinite extension. The Savitzky-Golay filter is of the type FIR. Formally, a causal filter can be described on the form

$$H(z) = \frac{b_0 + b_1 z^{-1} + \dots + b_m z^{-m}}{1 + a_1 z^{-1} + \dots + a_n z^{-n}} \quad (2.21)$$

which is the transfer function of the filter. It is expressed by the  $z$ -transform for discrete-time signals. If the denominator coefficients  $a_1, a_2, \dots, a_n = 0$  then  $H(z)$  is a FIR filter, while any  $a_i \neq 0$  results in a IIR filter [35].

What filter to choose is not trivial and there are numerous types of filters belonging to both groups. Generally, IIR filters are more computationally efficient and require lower orders to obtain equal performance as a FIR filter. However, due to

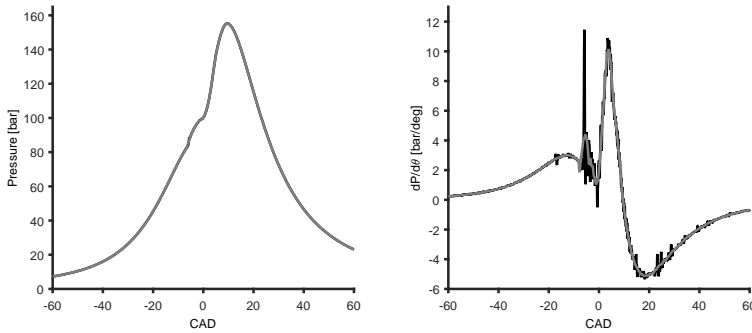


**Figure 2.3:** The effect of differentiating noisy pressure data compared to data filtered with a Savitzky-Golay low-pass filter.

the feedback (dependency on previous outputs) it is possible to get an unstable filter. Another effect of feedback is non-linear phase shift which is more difficult to compensate.

FIR filters are stable since there is no feedback and they have linear phase-shift. As stated earlier FIR filters require higher orders than IIR filters to achieve the same performance. However, if computational power or time is not an issue, it is possible to get almost any performance from a FIR filter. An IIR filter cannot be created with infinitely many poles ( $a_i$ ) due to the instability problem, hence their maximum performance is restricted.

In Figure 2.3 it is demonstrated how a Savitzky-Golay low-pass filter affects the pressure derivative. Note however that the smoothing has drastically decreased the peaks of the most rapid pressure changes. A trade-off must be found between noise suppression and loss of information. How much smoothing distortion is tolerable will depend on if the application emphasize qualitative or quantitative analysis of the HRR.

## 2.4.2 Sampling

Usually sampling is done uniformly in time. However, in the automotive industry it is very common to sample angle-based due to the engine cycle events being directly connected to crank angle. This approach complicates the signal processing as standard methods assume uniform time sampling. By synchronising sampling with the crank angle the frequency content gets dependent on engine speed. When designing a filter it is no longer possible to define a constant, optimal cutoff frequency as the signal bandwidth changes. A constant filter will only perform as expected in a small interval of the engine's operating range, assuming a somewhat constant speed. A way to overcome the problem is by using an adaptive filter with adjustable cutoff frequency. A simpler approach is to adjust the cutoff frequency to the operating point containing the highest (interesting) frequency content. The downside is of course that more noise might interfere at operating

points with lower frequencies, where the cutoff should have been set lower to attenuate the maximum amount of noise.

### 2.4.3 Aliasing

A phenomenon that might occur when sampling is *aliasing*. It happens when the sampled signal contains frequencies higher than the Nyquist frequency,  $\omega_N$ . It is defined as

$$\omega_N = \frac{\omega_S}{2} \quad (2.22)$$

where  $\omega_S$  is the sampling frequency. It states that the sampling frequency must be at least two times the bandwidth of the signal that is captured. Frequencies above  $\omega_N$  will be erroneously seen as lower frequency content and cause alias, i.e. distortion in lower frequency data. To eliminate the problem it is very important that the signal is low-pass filtered before it is sampled in the measurement setup, with the cutoff frequency at  $\omega_N$ . This is also known as an *anti-alias filter*.



# 3

---

## Data acquisition

The data required in this work was collected together with several other thesis workers. Therefore the collective experimental set-up is presented in this chapter combined with more specific information about the cylinder pressure transducer. Not all measurements listed in this chapter was actually used when developing the virtual sensors.

### 3.1 Experimental set-up

The engine used for the data acquisition was a Scania D13 inline six-cylinder diesel engine. The engine data is given in Table 3.1.

*Table 3.1: The geometric data of the Scania D13 engine.*

Parameter	Unit	Value
Engine displacement	dm <sup>3</sup>	12.74
No. of cylinders	-	6

The in-cylinder pressure sensors are of two types. The first one is the Kistler 7061B, mounted on cylinder one. It is a piezoelectric, water-cooled, high-precision sensor suited for thermodynamic measurements. The second sensor is the AVL GU24D, mounted on cylinder six. It is a piezoelectric, uncooled sensor. Both are flush mounted with the cylinder wall. They are known to have a very linear characteristic and high accuracy. See Table 3.2 for a short summary of the sensor specifications. The pressure signal is pegged to the MAP at IBDC.

An schematic overview of the sensor set-up can be seen in Fig. 3.1. There were two groups of data sets. The first group was continuously sampled with a high

**Table 3.2:** Sensor specifications of the Kistler 7061B and the AVL GU24D.

Sensor		7061B	GU24D
Range	bar	0...250	0...250
Sensitivity	pC/bar	≈80	45
Natural frequency	kHz	≈45	≈92
Linearity, all ranges	% FSO	≤ ±0.5	≤ ±0.3
Operating temperature range	°C	-50...+350	-40...+400
Load-change drift	bar/s	< ±0.5	< ±4

frequency and the other group contained averaged data. The continuously sampled signals are as follows:

- *Cylinder pressure*: This is measured on the first and sixth cylinders.
- *Crank angle encoder*: The CAD is measured using an optical sensor which gives a pulse every 0.5 degrees. The measurements are extrapolated at four points in between two pulses to yield a resolution of 0.1 degrees.
- *Intake manifold pressure*
- *Rail pressure*
- *Knock sensors*: The sensors are mounted on the exhaust side of the cylinder block on cylinder number one and six.
- *Needle lift*: The current to the fuel injector on cylinder one and six.

This below list includes the measurements which are averaged over one or several engine cycles.

- *Intake and exhaust temperatures*
- *Exhaust pressure*
- *Brake torque*: The output torque is measured as an average over an engine cycle. This is measured through the dynamometer.
- *NOx sensor*: This sensor measures NOx level in the exhaust gas but can also measure the oxygen level. This can be used to calculate  $\lambda_{exh}$  (air/fuel mixture).
- *Oil temperature*: Temperatures in the oil are measured on several positions on the engine, e.g. oil sump, piston gallery and temperature differences over auxiliary components.

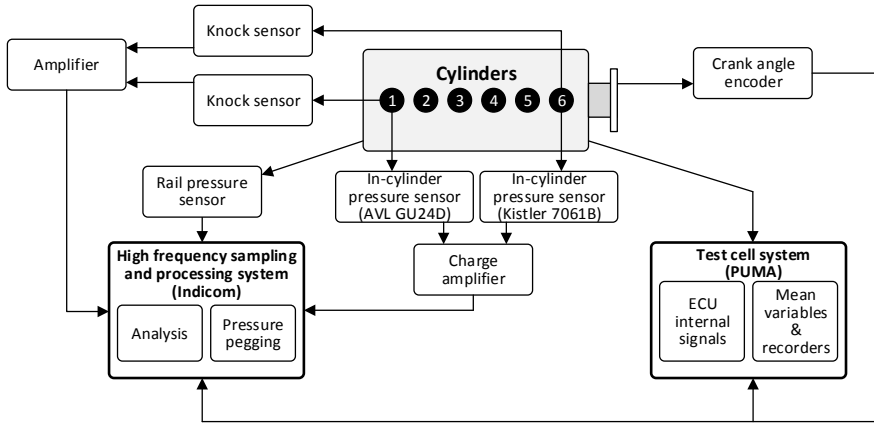


**Figure 3.1:** A schematic overview of the most significant parts of the test setup. The sampling was done with two systems; AVL's Indicom and Puma. Indicom handled the high frequency sampling of in-cylinder pressure, knock sensors and rail pressure. It also provided heat-release analysis which has been used as early validation of the correct implementation of the heat-release algorithm. Puma interfaced with the ECU and provided data from recorders sampling at lower frequencies, e.g. temperatures and exhaust pressures.

Some signals are model-based or available as demanded quantities within the ECU. Some of these signals is saved alongside the other data set and are listed below.

- SOI
- SOC
- $\theta_{CA10}$ ,  $\theta_{CA50}$ ,  $\theta_{CA90}$
- $\lambda_{exh}$
- Demanded amount of fuel in main and pilot injections

## 3.2 Data sampling

The data was sampled every 0.1 CAD and was the maximum resolution available. With such high resolution it was also possible to down-sample the signal either to test the virtual sensors with coarser sampling or get rid of high-frequency disturbances.

The ECU signals of interest were available as scalars on cycle-by-cycle basis.

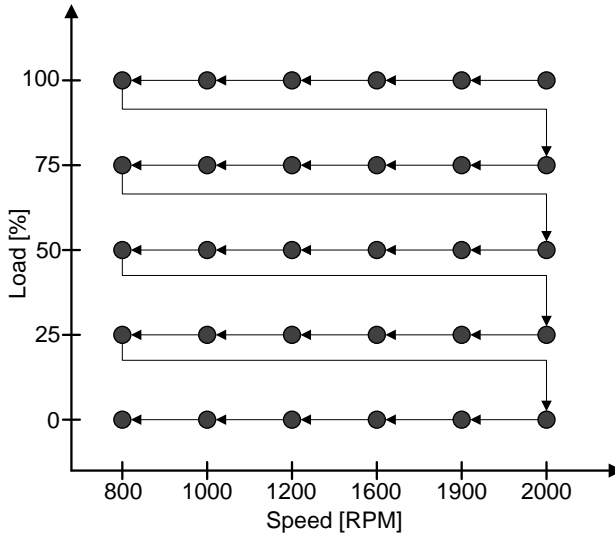


*Figure 3.2: Load and speed points that are tested. The speed is stepped through for every load, the load is then decreased, and the speed is changed again from high to low etc. The motoring cycles are not illustrated in this diagram.*

### 3.3 Experimental procedure

The tests were divided into stationary operating points, dynamic ramps, adjusted SOI and long term oil degradation tests.

**Stationary operating points** A point was considered stationary after two minutes of constant load and speed. Then 50 cycles was sampled before moving to the next operating point. The operating points of interest are illustrated in Fig. 3.2.

The testing procedure began at high load and high speed. After sampling was completed the speed was decremented while the load was unchanged. Then the sampling was repeated when the operating point had stabilised. When all speeds had been sampled the load was decremented one step and the speed was yet again changed from high to low. This procedure was repeated until all loads had been sampled at every specified speed.

The tests were done with two different fuels; Euro VI reference fuel with 7 % RME and B100 biodiesel with 100 % RME.

Motored cycles were done as a standard stationary measurement at each speed except no fuel was injected.

**Dynamic ramps** The ramps were performed in speed and in load. The ramp was done in a similar manner as before with the exception of a continuously varying load or speed. Each ramp was repeated three times. The tests cases were,

- Constant load, ramp in speed. This was made for a constant load of 50 %. The starting speed was 800 RPM and the slope of the ramp is 40 RPM/s over 5 seconds. The tests were repeated with a starting speed of 1200 RPM.
- Constant speed, ramp in load. The speed was held constant at 1200 RPM and the torque was ramped from 1200 Nm to 1700 Nm with 100 Nm/s. Then the ramp was done again with a speed of 1500 RPM and load ramp from 800 Nm to 1200 Nm, with a slope of 100 Nm/s.

**Adjusted SOI** During these tests the engine is kept at 75% load. The tests are made for two engine speeds, 1200 RPM and 1900 RPM. For these two cases the fuel injection timing is changed between 0,  $\pm 2$ ,  $\pm 10$  CAD.

**Oil temperature** The engine was running during nights to allow for more long term experiments of the oil degradation.



# 4

---

## Modelling

In this chapter the implementation phase is described, where the selection of methods and algorithms are described. The first section describes the signal processing of the cylinder pressure. In the following section the implemented heat-release models are shown and more specifically how the specific heat ratio  $\gamma$  was determined. The last section describes the algorithms of the virtual sensors.

When selecting a suitable method several (wanted) requirements were made:

1. Sufficient accuracy
2. Low sensitivity to noise
3. Minimum dependence on simulation models (e.g. to decide parameters)
4. Low computation cost

### 4.1 Signal processing of pressure sensor signal

The pressure data is of no use if the signal processing is insufficient. The effects being considered concerns the

- Signal noise reduction
- Absolute pressure referencing
- Zero-level drift
- Crank angle phasing

### 4.1.1 Constant filter techniques

As a first step constant filters were tested, due to the ease of implementation. Several filters were tested to evaluate which one performed satisfactorily. Tested filters was of type Butterworth, Savitzky-Golay and Chebyshev type 1.

It is common to get a phase shift when applying filters. Due to the importance of having pressure data synchronized with the CAD the phase shift must be compensated by reversing the phase-shift. This is fortunately not a difficult problem to solve due to the assumption that calculations are performed on one or more complete cycles. First of all it allows for non-causal filters, and secondly it is easy to compensate filters with non-linear phase shift (`filtfilt` command in MATLAB).

### 4.1.2 Filter with adaptive cutoff frequency

To combat the weaknesses of constant filter techniques a second filtering method was implemented which is based on [36]. It makes use of the Discrete Fourier Transform (DFT) together with statistics to automatically set an, in some sense, optimal cutoff frequency. The filtering is done in five steps:

1. Collect data from consecutive cycles at some operating point.
2. Transform the data series with the DFT.
3. Split data into harmonics and noise frequencies.
4. Compare harmonics and noise to decide the point where the signal-to-noise ratio has deteriorated to the point where the signal cannot be clearly distinguished from noise.
5. Cut off frequencies above the decided point and perform an inverse DFT to get the low-pass filtered, angle (time) domain data.

The sampled cylinder pressure data is transformed forming  $n_c \cdot n_s$  complex numbers, where  $n_c$  and  $n_s$  is the number of cycles and number of samples in one cycle, respectively.

The DFT of a signal  $u(kT)$  is defined as

$$U_N(i\omega) = T \sum_{k=1}^N u(kT)e^{-i\omega kT} \quad (4.1)$$

where  $N$  is the total number of samples. This means that the DFT describes the frequencies  $\omega_k = \frac{2\pi}{T} \cdot \frac{k}{N}$ , for  $k = 1, \dots, N$ , and correspondingly a *frequency resolution* of  $\frac{2\pi}{T \cdot N}$ . With  $N = n_c \cdot n_s$  and  $T^{-1} = \frac{\omega_s}{2\pi}$ ,

$$\omega_k = \frac{k}{n_c \cdot n_s} \omega_s = \frac{k}{n_c} \omega_0 \quad k = 0, \dots, n_c \cdot n_s - 1 \quad (4.2)$$

or, equivalently

$$f_k = \frac{k-1}{n_c} f_0 \quad k = 1, \dots, n_c \cdot n_s \quad (4.3)$$

where  $\omega_0$  and  $f_0$  is the fundamental frequency of the thermodynamic cycle.

If only one cycle is transformed ( $n_c = 1$ ) the frequency resolution would be equal to the fundamental frequency. If e.g.  $n_c = 50$  the resolution is improved by an equal amount. This means that every 50th frequency bin will correspond to a harmonic  $S_k$  and the 49 bins succeeding the harmonic is considered as noise  $N_{k,m}$  related to it. It can be denoted as

$$\{S_k, N_{k,m}\} \quad \text{with} \quad \begin{cases} k = 1, \dots, n_s \\ m = 1, \dots, n_c - 1 \end{cases} \quad (4.4)$$

The real and imaginary part in each frequency is considered as a separate independent variable with a normal distribution, where

$$\begin{aligned} S_k^{Re} &\sim N(\mu_k^{Re}, \sigma_k^{Re}) \\ N_k^{Re} &\sim N(0, \sigma_k^{Re}/\sqrt{n_c-1}) \\ S_k^{Im} &\sim N(\mu_k^{Im}, \sigma_k^{Im}) \\ N_k^{Im} &\sim N(0, \sigma_k^{Im}/\sqrt{n_c-1}) \end{aligned} \quad (4.5)$$

where  $N_k$  is the mean value of the  $n_c - 1$  noise frequencies related to harmonic  $k$ . The harmonics and noise is assumed to be affected by the same errors so both have a standard deviation based on  $\sigma_k^{Re}$

To determine where to set the cutoff frequency, a statistical test is performed to define the point where the harmonic cannot be clearly separated from the noise. This can be done by using confidence intervals:

$$\begin{aligned} (S_k^{Re} - N_k^{Re}) \pm \hat{\sigma}_k^{Re} \cdot t_{n_c-2}^{\alpha/2} \sqrt{n_c/(n_c-1)} \\ (S_k^{Im} - N_k^{Im}) \pm \hat{\sigma}_k^{Im} \cdot t_{n_c-2}^{\alpha/2} \sqrt{n_c/(n_c-1)} \end{aligned} \quad (4.6)$$

where  $S_k, N_k$  is the sample mean of harmonics and noise,  $\hat{\sigma}_k$  is the sample variance and  $t_{n_c-2}^{\alpha/2}$  is the  $t$ -value of a Student's distribution with  $n_c - 2$  degrees of freedom and probability  $1 - \alpha$ .

A Hann window is applied to this interval

$$\begin{aligned} S_k^{filt} &= \sum_{k=1}^{n_c \cdot n_s} h_k \cdot S_k \\ h_k &= \begin{cases} 1 & k < k_1 \\ \cos(\frac{\pi}{2} \cdot \frac{k-k_1}{k_2-k_1}) & k_1 \leq k \leq k_2 \\ 0 & k > k_2 \end{cases} \end{aligned} \quad (4.7)$$

which gives a transition from full amplitude ( $h_k = 1$ ) to zero ( $h_k = 0$ ).

Finally the inverse DFT returns the pressure signal to angle (time) domain, the result being an averaged, low-pass filtered signal with noise attenuation from harmonic  $k_1$ .

### 4.1.3 Cylinder pressure sensor model

In research and development well-calibrated and high-accuracy, piezoelectric pressure sensors are typically in use. Piezoelectric sensors' inherent weakness are offset drifting. In a production vehicle however, lower accuracy sensors will be used of piezoresistive or optical type. Not only offset are of concern but also gain errors resulting in the sensor model

$$p_m = kp + p_{bias} \quad (4.8)$$

where  $k$  is the gain and  $p_{bias}$  is the constant offset error. The gain will be considered as constant for a set of 50 cycles at a specific operating point while the offset is assumed to change between two consecutive cycles. The problem of deciding both gain and offset uniquely can be divided into two parts by careful selection of estimation intervals. At low pressures offset is typically the major source of error while at high pressures gain errors are the most significant. Offset estimation is consequently done at low pressure, every cycle, by either pegging it to intake manifold pressure or utilising a least-squares approach with a polytropic model. Employing the assumption of a polytropic process the pressure is related, in absence of combustion, by

$$(p_m - p_{bias})V^\kappa = (p_{m,0} - p_{bias})V_0^\kappa \quad (4.9)$$

where  $p_{m,0}$  and  $V_0$  are measurements at some reference level. Rewriting the expression one gets an expression for  $p_{bias}$  as

$$p_{bias} = \frac{1}{1 - \left(\frac{V}{V_0}\right)^\kappa} \left[ p_{m,0} - p_m \left(\frac{V}{V_0}\right)^\kappa \right] \quad (4.10)$$

which can be solved by linear least-squares (LLS) if  $\kappa$  is assumed to be known and several pressure samples are available. If  $\kappa$  is unknown a non-linear least-squares (NLLS) similar to the algorithm presented in Section 4.1.5 is required.

Gain error is estimated in two ways, the first is by using a polytropic model but changing  $\gamma$  at every sampling point by using temperature and one of the  $\gamma$ -models presented in Section 4.2.2. The second one utilises the gross heat-release model, Eq. (4.21), but with  $\frac{dQ_{gross}}{d\theta} = 0$ . Also here  $\gamma$  is changed at every step. The pressure trace is estimated using IVC conditions as starting point and ending at  $-20^\circ$  ATDC. Gain is then estimated as the  $k$  that minimises the error between the measured and estimated pressure.

### 4.1.4 Compensation for zero-level drift

Compensation of intra-cycle zero-level drift has not been implemented due to the experimental data showing no obvious signs of drifting. This is in agreement with the sensor specification data in Tab. 3.2. The AVL GU24D has at most 4

bar/s of load-change drift which is eight times higher than the Kistler 7061B. The slowest cycle measured was 800 RPM, and pegging the pressure at IBDC effectively means 400 RPM. This translates to pressure pegging with 6.67 Hz or every 0.15 seconds, i.e. < 0.7 bar over a complete four-stroke cycle. The pressure drift is considered negligible.

#### 4.1.5 Estimating TDC position

Accurate calibration of TDC position is vital for the estimation of IMEP. The IMEP estimation error is in the range 3 % to 10 % per degree of error in phase [37]. The crank angle phasing error must be within  $0.1^\circ$  to ensure an IMEP error below 1 %.

The investigation of previous research proved that TDC estimation is difficult, and that the most accurate methods are quite computation intensive. The demands described in the introduction to this chapter are difficult to fulfil at the same time. Several methods either depend on simulations to decide parameters needed in the estimation model [16, 38] or to simulate a thermodynamic cycle [14]. They all fail on requirement number 3 and in some sense on number 4 due to extensive simulations. The simulations are also very dependent on engine specifications and therefore not very flexible.

The selected method follows the suggestions in [29]. It uses the net heat-release model to decide specific heat ratio  $\gamma$ , heat power  $k$  and TDC offset  $\theta_0$ . The strong assumption in this model is a constant heat power during a motoring cycle. However, it is resilient to noise since it uses a range of points, it requires no separate simulation to decide model parameters and it is easy to deploy on any engine. The first point, high accuracy, is difficult to confirm without a proper way of simulation. According to the author it performs well and can estimate TDC to within  $0.1^\circ$  of the true TDC in a laboratory setting.

With  $\frac{dQ_{net}}{d\theta} = k$ , Eq. (2.2) can be rewritten as

$$\frac{dp}{d\theta} = k(\gamma - 1) \frac{1}{V(\theta)} - \gamma p(\theta) \frac{dV}{d\theta} \frac{1}{V(\theta)} \quad (4.11)$$

Inserting the phasing error  $\theta_0$  in Eq. (4.11)

$$\frac{dp}{d\theta} = k(\gamma - 1) \frac{1}{V(\theta + \theta_0)} - \gamma p(\theta) \frac{dV(\theta + \theta_0)}{d\theta} \frac{1}{V(\theta + \theta_0)} \quad (4.12)$$

Given  $\theta_0$  the problem is linear in  $C = k(\gamma - 1)$  and  $\gamma$ . By forming  $x = [C \quad \gamma]^T$ ,  $y_i = \frac{dp(\theta_i)}{d\theta}$  and  $\phi_i = \left[ \frac{1}{V(\theta_i + \theta_0)} \quad p(\theta_i) \frac{dV(\theta_i + \theta_0)}{d\theta} \frac{1}{V(\theta_i + \theta_0)} \right]$  the problem can be written on the form

$$y_i = \phi_i x \quad (4.13)$$

With  $i$  points the output and regressor matrix is constructed as

$$Y = \begin{bmatrix} y_1(\theta_1|\theta_0) \\ y_2(\theta_2|\theta_0) \\ \vdots \\ y_N(\theta_N|\theta_0) \end{bmatrix} \quad (4.14)$$

$$\Phi = \begin{bmatrix} \phi_1(\theta_1|\theta_0) \\ \phi_2(\theta_2|\theta_0) \\ \vdots \\ \phi_N(\theta_N|\theta_0) \end{bmatrix} \quad (4.15)$$

with the solution

$$\hat{x} = \Phi^+ Y \quad (4.16)$$

With a new estimation  $\hat{x}$  the phasing error  $\theta_0$  can be calculated by solving the NLLS. It is solved by using `lsqnonlin` in MATLAB's Optimization Toolbox. The function utilises a Trust-region method and is provided with a cost function  $V_N$  and an analytical expression of the gradient  $\nabla V_N$ . The cost function  $V_N$  and gradient  $\nabla V_N$  is constructed as

$$V_N = \frac{1}{2}(Y - \Phi\hat{x})^T(Y - \Phi\hat{x}) = \frac{1}{2}R^T R \quad (4.17)$$

$$\nabla V_N = R^T \frac{\partial R}{\partial \theta_0} = R^T \frac{\partial(-\Phi\hat{x})}{\partial \theta_0} = -R^T \frac{\partial \Phi}{\partial \theta_0} \hat{x} = -R^T J \hat{x} \quad (4.18)$$

where

$$J = \begin{bmatrix} \frac{\partial \phi_1}{\partial \theta_0} \\ \frac{\partial \phi_2}{\partial \theta_0} \\ \vdots \\ \frac{\partial \phi_N}{\partial \theta_0} \end{bmatrix} \quad (4.19)$$

The updated  $\theta_0$  is inserted into Eq. (4.16) to compute a new  $\hat{x}$  which is inserted into Eq. (4.17) and (4.18), and  $\theta_0$  is updated again etc. The algorithm iterates until the solution converges.

The benefit of separating the problem is that the NLLS problem only have one unknown, decreasing the complexity and number of iterations to get a solution.

To validate correctness of phase, one way is to look at the p-V diagram. The compression and expansion lines should not cross each other at TDC in a motoring operation [3]. Another validation method is to estimate the TDC position at different speeds and cycles and look at the deviation cycle-to-cycle and between operating points. If the estimation model captures all phenomena the TDC position should be equal in all cases [39].

## 4.2 Heat-release model

How to model the heat-release is dependent upon the goal of the analysis. If absolute measures are needed, e.g. to be used in simulations, the gross heat-release is appropriate which is given in Eq. (2.1). One way of modelling the heat transfer is by the well-known Woschni relation [11] which is very common in research. A down-side though is the inaccuracy of the model, or at least to say with confidence when it describes the heat transfer accurately [10]. That is however not restricted to Woschni's model but all heat transfer models trying to describe a very complex process with a simplified, semi-empirical formula.

In an production vehicle setting with less accurate measurement and restricted processing power a high complexity model might not produce the expected accuracy, if it is even possible to implement. No matter the complexity of the model there will always be some parts of the combustion that are not fully described when employed on a real engine.

To compare how different complexities affect the performance of combustion analysis two models have been tested; the net heat-release formulation described in Eq. (2.2),

$$\frac{dQ_{net}}{d\theta} = \frac{\gamma}{\gamma-1} p \frac{dV}{d\theta} + \frac{1}{\gamma-1} V \frac{dp}{d\theta} \quad (4.20)$$

and the gross heat-release described in Eq. (2.1), but with crevice effects neglected resulting in losses only from heat transfer

$$\frac{dQ_{gross}}{d\theta} = \frac{\gamma}{\gamma-1} p \frac{dV}{d\theta} + \frac{1}{\gamma-1} V \frac{dp}{d\theta} + \frac{dQ_{ht}}{d\theta} \quad (4.21)$$

where

$$\frac{dQ_{ht}}{d\theta} = \frac{dQ_{ht}}{dt} \cdot \frac{1}{\omega_e} = h_c A (T - T_w) \cdot \frac{1}{\omega_e} \quad (4.22)$$

The parameter  $h_c$  is parametrised using Woschni's formula [11].

The downside of the net heat-release approach is of course that no losses are taken into account. According to Heywood [5], the exclusion of heat transfer mainly affects the maximum amount of heat released, not the shape of the heat-release. In what extent heat-release is affected considering the effect of assumptions, tolerances etc., and in the end the effect on combustion parameter estimations, will be presented in Chapter 5. Of special interest is the effect of typical issues associated with real engines; ageing, fuel type, engine variations and measurement accuracy.

### 4.2.1 Calculation of pressure derivative, volume and area

Pressure is differentiated by a middle-point scheme,

$$\frac{dp}{d\theta} = \frac{p(\theta_{i+1}) - p(\theta_{i-1})}{\theta_{i+1} - \theta_{i-1}} \quad (4.23)$$

which is important to prevent phase shift with respect to pressure, volume, and volume derivative. The volume and its derivative is analytically calculated by

$$V(\theta) = V_c + \frac{V_d}{2} \left( R + 1 - \cos \theta - \sqrt{R^2 - \sin^2 \theta} \right) \quad (4.24)$$

$$\frac{dV}{d\theta} = \frac{V_d}{2} \sin \theta \left( 1 + \frac{\cos \theta}{\sqrt{R^2 - \sin^2 \theta}} \right) \quad (4.25)$$

where  $V_c$  is the clearance volume,  $V_d$  is the cylinder displacement volume and  $R = \frac{l}{r}$  is the ratio between the connecting rod length,  $l$ , and crank radius,  $r$ .

The instantaneous combustion chamber area, required in the heat transfer model, is calculated as

$$A(\theta) = (1 + A_p)\pi \frac{B^2}{4} + \pi B \frac{L}{2} \left( R + 1 - \cos \theta - \sqrt{R^2 - \sin^2 \theta} \right) \quad (4.26)$$

where  $A_p$  is the piston area coefficient. Since the piston area is far from a flat disc in the tested engine the area has been set 40% higher which gives  $A_p = 1.4$ .

### 4.2.2 Specific heat ratio

A major part of the chosen heat-release model involves the calculation of the specific heat ratio  $\gamma$ . It is commonly considered as the most effecting parameter in heat-release calculations. Several approaches were tested, including constant value by some arbitrary selection, a linear model in temperature and a model based on the NASA polynomials [40] which is a function of  $\lambda$  and temperature.

To see how large impact  $\gamma$  has on the final combustion parameter estimations in a production vehicle, a comparison has been made with all suggested models. Both models use a one-zone mean charge temperature as input, given from

$$T(\theta) = \frac{T(\theta_{ref})}{p(\theta_{ref})V(\theta_{ref})} p(\theta)V(\theta) \quad (4.27)$$

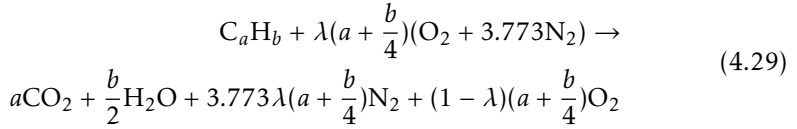
which is derived from the ideal gas law. The angle  $\theta_{ref}$  is the angle at IVC where  $T \approx T_{boost}$  and  $p \approx p_{boost}$ .

The NASA polynomials gives the value  $c_p$  of a species at a specified temperature  $T$  by the empirical equation

$$\frac{c_p}{R} = a_1 T^{-2} + a_2 T^{-1} + a_3 T^0 + a_4 T^1 + a_5 T^2 + a_6 T^3 + a_7 T^4 \quad (4.28)$$

where the coefficients  $a_1 \dots a_7$  are given by NASA Thermochemical tables. The cylinder charge is simplified to only consist of air and burned gases, and the fuel is modelled as a reaction between hydrocarbon and oxygen giving the simplified

reaction



The  $c_p$  value of every species is calculated based on current temperature and the amount of moles of each species. Finally the average specific heat  $\bar{c}_p$  of the contents is estimated by interpolating between burned gases and air with the MFB trace calculated with a constant  $\gamma$ ,

$$\bar{c}_p = (1 - x_b) c_{p,air} + x_b c_{p,b} \quad (4.30)$$

Finally, assuming an ideal gas, the specific heat ratio is

$$\gamma = \frac{\bar{c}_p}{\bar{c}_v} = \frac{\bar{c}_p}{\bar{c}_p - R} \quad (4.31)$$

In the linear approach, the  $\gamma$ -model is divided in two linear parts. The first one describes compression of air while the second describes the combustion. It is written on the same form described by Gatowski et al. [4].

$$\gamma_1(T) = \gamma_{1,300} + b_1(T - 300) \quad (4.32)$$

$$\gamma_2(T) = \gamma_{2,300} + b_2(T - 300) \quad (4.33)$$

Finally  $\gamma$  is calculated by interpolating between the two models in the same manner as before,

$$\gamma = (1 - x_b) \gamma_1 + x_b \gamma_2 \quad (4.34)$$

Common simplifications in both models are the neglecting of added mass from fuel injection and change of substance (amount of moles) during combustion.

The linear models are fitted to data from CHEPP [41], created by Lars Eriksson at Linköping University. It is a program package for MATLAB that calculates chemical equilibrium and thermodynamic properties of reactants and products of a combustion reaction between fuel and air.

### 4.2.3 Algorithm

Heat release is straightforward to compute given the models in Eq. (4.20)-(4.21) and a correctly phased pressure and volume trace. See Fig. 4.1 for an illustrative description of the algorithm. The steps can be summarised as:

1. Collect  $N$  complete cycles of pressure data  $p_k$ ,  $k = 1 \dots N$ , at a stationary operating point
2. Calculate the average pressure  $\bar{p} = \frac{1}{N} \sum_{k=1}^N p_k$
3. Run  $\bar{p}$  through a low-pass filter to get  $p_{filt}$

4. Calculate the pressure derivative  $\frac{dp_{filt}}{d\theta}$
5. Calculate the cylinder volume trace  $V$ , its derivative  $\frac{dV}{d\theta}$  and  $A$  from Eq. (4.24), (4.25) and (4.26)
6. Insert  $\bar{p}$  and  $V$  into Eq. (4.27) to get  $T$
7. Get an approximate MFB trace by normalising the cumulative heat-release from Eq. (4.20), calculated with a constant  $\gamma$
8. If no  $\lambda$  is available, calculate it from cylinder pressure
9. Calculate  $\gamma$  from Eq. (4.31) from a selected model or set it constant.
10. Insert  $p_{filt}$ ,  $\frac{dp_{filt}}{d\theta}$ ,  $V$ ,  $\frac{dV}{d\theta}$ ,  $A$ ,  $\gamma$  into Eq. (4.20)-(4.21) to get  $\frac{dQ_{net}}{d\theta}$  and  $\frac{dQ_{gross}}{d\theta}$

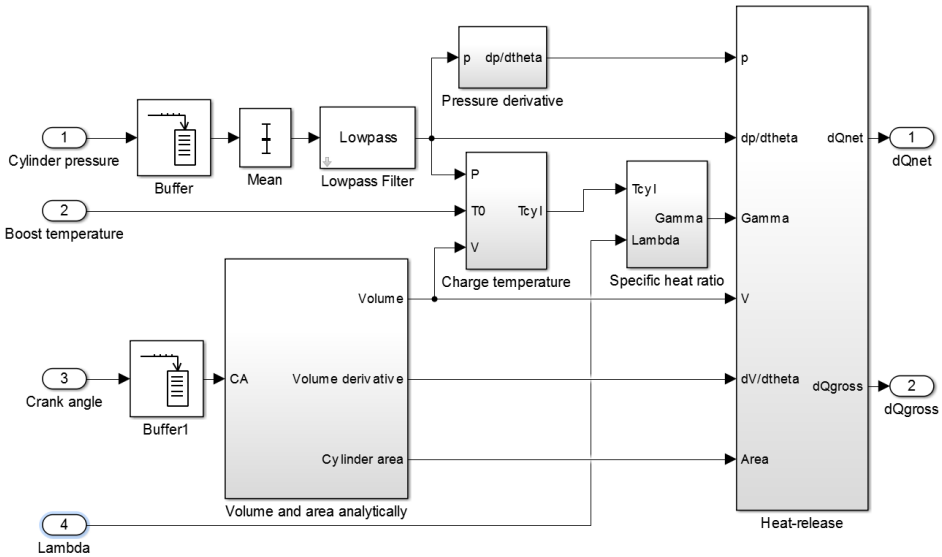


**Figure 4.1:** A flowchart description of the algorithm to calculate the heat-release. The calculations are done on averaged pressure data.

### 4.3 Heat-release parametrisation by Vibe functions

A common way is to apply some kind of distribution function, e.g. normal or gamma distributions, to represent the burned fraction trace. One of the most well-known relationships is the Vibe function [42],

$$x_b = 1 - \exp \left[ -a \left( \frac{\theta - \theta_{ign}}{\theta_d} \right)^{m+1} \right] \quad (4.35)$$

where  $\theta$ ,  $\theta_{ign}$  and  $\theta_d$  are the instantaneous, ignition and duration angles respectively. Parameters  $a$  and  $m$  are design parameters. The chosen parametrisation is in fact over-parametrised in  $a$  and  $\theta_d$  which means at least one of them must be set constant as suggested by e.g. Eriksson and Nielsen [28]. Parameter  $a$  can be calculated analytically from Eq. (4.35) assuming a specific fraction  $x_b$  has burned at the end of the combustion duration  $\theta_d$ . The correlation is  $a = -\ln(1 - x_b)$ .

In order to accurately reconstruct the heat-release in diesel engines several Vibe functions are required. Investigations performed by the author showed that a minimum of two functions are needed in order describe the main combustion event; one for premixed combustion, and one for diffusion and late combustion. One Vibe function must be added for each additional injection. In this work, a decision was made to parametrise double-injection strategies consisting of one pilot and one main injection. This was by far the most common multi-injection strategy for the specific testing engine.

The main combustion event was fitted with the following function

$$x_b = \beta x_{b1} + (1 - \beta)x_{b2} \quad (4.36)$$

where  $x_{b1}$  and  $x_{b2}$  have their own set of parameters, in total nine parameters including  $\beta$ . When pilot injections occurs it is fitted with a separate Vibe function according to Eq. (4.35), for a total of 13 parameters.

A problem that magnifies with increasing number of Vibe functions is the risk of bad solutions. Care must be given to the boundary and initial conditions in the optimisation problem. To decrease the complexity of the optimisation  $a = 6.907$  for all functions, corresponding to 99.9% burned fuel. Parameter  $\theta_d$  in  $x_{b2}$  was set to  $120^\circ$  since the diffusion (or late combustion) has a long tail often ending not very far from EVO. If this parameter is a little off it will not have a huge impact on the curve fit since the trailing combustion do not constitute a large part of the total heat released.

Initial values of the remaining parameters was set to the values estimated from the heat-release constructed from measurements. The optimisation is done with `lsqnonlin` which uses the Trust-region algorithm when provided with boundary conditions.

## 4.4 Virtual sensors for the combustion parameters

In this section the algorithms are presented for the combustion parameters. Many of them are implemented approximately as presented in the theory chapter (Section 2.2.1).

### 4.4.1 Maximum pressure

Due to substantial noise or wavelets affecting the signal around TDC, a decision was made to perform a least-squares fit of a second order polynomial

$$p_{model} = a\theta^2 + b\theta + c \quad (4.37)$$

in a short interval of  $\pm 4^\circ$  surrounding the raw maximum pressure position.

The problem was constructed as

$$Y = \begin{bmatrix} p(\theta_1) \\ p(\theta_2) \\ \vdots \\ p(\theta_N) \end{bmatrix}, \quad \Phi = \begin{bmatrix} \theta_1^2 & \theta_1 & 1 \\ \theta_2^2 & \theta_2 & 1 \\ \vdots & \vdots & \vdots \\ \theta_N^2 & \theta_N & 1 \end{bmatrix}, \quad x = \begin{bmatrix} a \\ b \\ c \end{bmatrix} \quad (4.38)$$

$$\hat{x} = \Phi^+ Y \quad (4.39)$$

Thus the maximum is estimated by inserting  $a$  and  $b$  into the analytical solution  $\frac{dp_{model}}{d\theta} = 0$  and solving for  $\theta$ ,

$$\theta = -\frac{b}{2a} \quad (4.40)$$

and lastly inserting  $\theta$  into Eq. (4.37) to get  $p_{max}$ .

### 4.4.2 Compression ratio estimation

For satisfactory heat-release analysis, the accurate determination of compression ratio is vital. Simply using manufacturer specifications might not be enough due to mechanical tolerances causing variability in compression ratio from engine-to-engine, and even cylinder-to-cylinder [3, 39]. According to Klein [30] it is, second to  $\gamma$ , the most important parameter in accurate heat-release analysis.

It has been difficult to find a way of estimating compression ratio in a robust way. Most methods proposed by researchers uses NLLS of varying complexity by simultaneously predicting pressure sensor offset and/or crank angle phase. The more computationally efficient algorithms show biased estimates and decreasing accuracy with higher compression ratios. The most accurate estimator is based on the gross heat-release model, however it is very expensive [43].

The selected model is based on the variable projection method in [43] which shows the most promising results of the faster algorithms. It has fast convergence and the NLLS is separable and is solved in the same way as TDC position

(see Section 4.1.5). The problem is structured as

$$r(\theta) = \ln p(\theta) - [C - \kappa \cdot \ln(V_d(\theta) + V_c)] \quad (4.41)$$

where  $C$  is a constant,  $V_d$  is the displacement volume and  $V_c$  is the clearance volume. It is written on the same form as earlier, with  $x = [C \quad \kappa]^T$ ,  $y_i = \ln p(\theta)$  and  $\phi_i = [1 \quad \ln(V_d(\theta) + V_c)]$ . Compression ratio is calculated by using the estimated  $V_c$  in Eq. 2.14.

One way to validate the correctness of clearance volume is to look at the logarithmic p-V diagram in a motoring cycle and make sure that the compression and expansion lines are approximately straight. An error shows up as a curvature of these lines close to TDC [3].

### 4.4.3 SOC and ignition delay

Knowledge of SOC is of importance when estimating the ignition delay during engine operation, which in turn can be used to adjust the SOI positioning. It is also one of the parameters in the Vibe function.

SOC can be detected in the heat-release analysis as described in Section 2.2.1. However, there are advantages of being able to detect it without a full thermodynamic analysis, one example being computational cost.

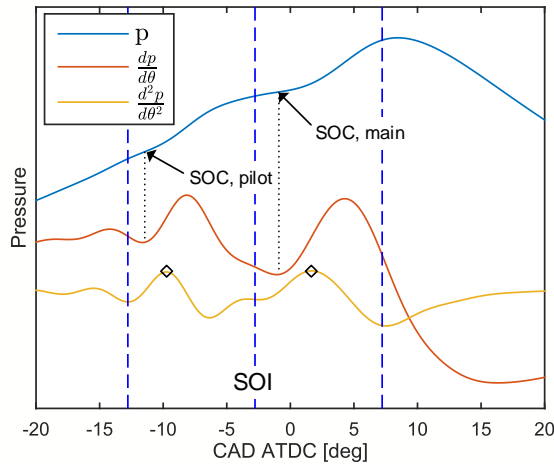


**Figure 4.2:** Visual overview of the SOC algorithm. The vertical dashed lines indicate the two search intervals and the diamonds indicate the local maxima of the second pressure derivative. It can be clearly seen that the local maxima occurs shortly after SOC. The dotted lines indicate the local minima of the first pressure derivative. It coincides well with the SOC, which occurs just before the accelerated pressure increase.

The pressure build-up in the cylinder arises from two sources; the compression stroke and the combustion of fuel. When the fuel ignites the pressure increases

very rapidly. By exploiting the knowledge that the added heat from the combustion results in an additional pressure increase, the latter can be used directly to find the ignition point.

The implemented algorithm uses the first and second derivative of the cylinder pressure to decide the point of ignition. It finds SOC for both pilot and main injections by searching for  $\left(\frac{d^2p}{d\theta^2}\right)_{max}$  in two separate intervals. The intervals are  $\theta \in [\theta_{SOI} - 10^\circ, \theta_{SOI}]$  for the pilot injection and  $\theta \in [\theta_{SOI}, \theta_{SOI} + 10^\circ]$  for the main injection. When the maximum point is found, the algorithm searches for the closest local minimum in  $\frac{dp}{d\theta}$ , which was defined as the point of ignition. An illustration is shown in Fig. 4.2. Theoretically it is sufficient to use the first pressure derivative to find the local minimum, but when implemented the algorithm failed in operating points with increased noise. By introducing the second derivative the estimations was more accurate.

When SOC is found the ignition delay can be calculated from the difference  $\tau = \theta_{SOC}^{main} - \theta_{SOI}^{main}$ . Ignition delay for pilots are not calculated.

#### 4.4.4 IMEP and indicated torque

IMEP is calculated as the net IMEP, i.e. during the whole four-stroke cycle. By reformulating Eq. (2.12) in Section 2.2.1 to a discrete equation, the calculation becomes

$$IMEP_{net} = \frac{\theta_{res}}{V_d} \sum_{k=1}^N p(\theta_k) \cdot \frac{dV(\theta_k)}{d\theta} \quad (4.42)$$

where  $\theta_{res}$  is the sampling resolution in crank angles,  $N$  is the number of samples and  $\theta_k \in [-360^\circ, 360^\circ]$ .

The calculation should be done *after* crank angle phasing correction since IMEP is very sensitive to phasing errors between pressure and volume.

Indicated torque is calculated as presented in Eq. 2.13.

#### 4.4.5 CAx and combustion duration

Estimation of CAx is performed as described in Eq. (2.7)-(2.10) in Section 2.2.1, with the only modification that  $\max(Q)$  is replaced by  $\max(Q_{tot}) = Q_{max} - Q_{min}$ , because  $Q < 0$  between SOI and SOC due to fuel evaporation.

Combustion duration is not calculated according to Eq. (2.11). Instead of  $\theta_{CA90}$  as the estimated end of combustion (EEOC) it is approximated as the point where  $\frac{dQ}{d\theta}$  is less than 3% of  $\left(\frac{dQ}{d\theta}\right)_{max}$ . The reason is that this provided a more stable estimation of EOC compared to  $\theta_{CA90}$  which depends on noise and small offsets in the heat-release during late combustion. With a well-functioning SOC algorithm  $\theta_{CA10}$  was replaced by  $\theta_{SOC}$  resulting in,

$$\theta_d = \theta_{EEOC} - \theta_{SOC} \quad (4.43)$$

as the new estimated combustion duration algorithm.

#### **4.4.6 Engine efficiency**

Efficiency is calculated as presented in Eq. 2.17.

#### **4.4.7 Heating value of fuel**

Typically the lower heating value for standard diesel is used. This will of course give an error when using another fuel as biodiesel which has a lower heating value. Without a way to estimate the heating value in a production vehicle the heating value is not changed during calculations.



# 5

---

## Results

In this chapter the results of a tolerance analysis is described which tries to assess the impact of different errors on combustion parameter estimations. Unfortunately, everything cannot be tested, but the issues addressed are the ones most probable to exist in a production vehicle. This includes sensor errors, lower accuracy measurement equipment, fuel types, ageing and individual variances. Since the measurement data is performed in a well-calibrated, high-performance sensor environment this is considered as the reference data. The nominal values are taken directly from these measurements. Nominal values for the engine geometry is taken from the manufacturers specification sheet. Errors are then injected one-by-one to see the effect on the estimations.

The analysis is divided into three parts; signal processing, estimations from measured pressure and finally an assessment of the Vibe parametrisation. The first one investigate the need for, and ability of, the algorithms to correct sensor bias, gain and crank angle phasing. In the second part an investigation is made on how typical errors affect estimations made directly from a measured pressure signal. Part three validates the ability of the selected heat-release parametrisation to describe the combustion process in a Diesel engine.

Results are given in terms of RMSE and maximum deviation at each operating point. Confidence bounds are not possible to show since the 50 cycles available are averaged before estimations begin. To get confidence bounds more cycles must be sampled in the test bench which was not possible at the time of testing.

In the following figures results are plotted against operating point. To keep the notation short a numbering notation has been applied according to Table 5.1. To summarise, every set of four numbers are one load with decreasing engine speed. The load is a percentage of the engine's maximum torque at the specified speed.

**Table 5.1:** Explanation of the operating point numbering in the following results.

Load [%]	Speed [RPM]			
	2000	1600	1200	800
100	1	2	3	4
75	5	6	7	8
50	9	10	11	12
25	13	14	15	16

## 5.1 Filtering

The adaptive filtering approach that was presented in Section 4.1.2 has been tested but with discouraging results. The filter consistently set the cutoff frequency too high, resulting in useless heat-release calculations destroyed by noise. Due to time constraints, the algorithm could not be modified from the presented framework.

## 5.2 Cycle-to-cycle variations

To get an indicator of how many cycles are needed in the averaging process, a statistical approach was used where the sample mean of four combustion parameters are plotted with  $3\sigma$  which is equivalent to 99% confidence intervals. In Fig. 5.1 the sample mean and confidence intervals are plotted against number of cycles averaged. The absolute values have been normalised by the average value from all 50 cycles. The tests have been performed over a wide range of operating points with consistent results of 25-30 cycles as an appropriate number. After this point, no great improvement is made by collecting more cycles.

## 5.3 Absolute pressure referencing

Pressure pegging to intake manifold pressure seems to be very accurate given a correct measurement in the intake manifold. A common problem that usually arise is speed dependent effects due to tuned intake runners, more specifically standing waves [30]. According to Fig. 5.2 the tested engine shows no such effects. The pressure is pegged at  $-180^\circ$  ATDC and this seems to be the best point to do so because the pressure difference is at the most stable point around that angle. Because of the noise superimposed on the signal it seems though as the accuracy is limited to the noise amplitude when pegging to a single point, see Fig 5.3.

The RMSE value has been calculated by averaging the pressure signal measurements in the range  $-185^\circ$  to  $-175^\circ$  ATDC. The polytropic model is not able to estimate the true pressure level at the same accuracy. Note however the sawtooth shape which has been identified as originating from choosing a constant  $\gamma$ . By

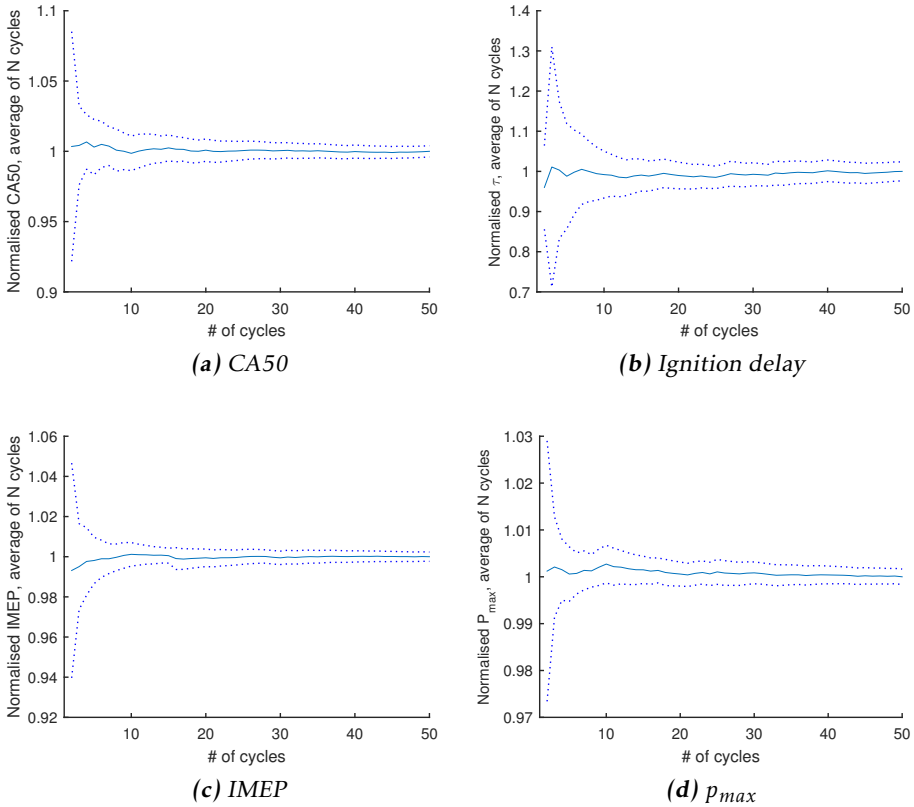


**Figure 5.1:** Four different combustion parameters and shown in (a)-(d). All parameters show no apparent improvement in confidence level after 25-30 cycles averaged.

adjusting  $\gamma$  in the range [1.37 ... 1.41] the error can be decreased. It was found that  $\gamma$  must be decreased with lower speeds. This tuning is most probably engine specific which is a step that must be minimised in a CLCC implementation.

The intake manifold pressure sensor is assumed to have a total accuracy of  $\pm a$  bar in a small interval around atmospheric pressure. This accuracy is not easily matched with a polytropic model with noisy pressure signals. It will be even more difficult when using production cylinder pressure sensors. To get equivalent performance with a polytropic pegging method  $\gamma$  has to be adjusted with speed which is probably engine specific. Therefore pegging to intake manifold pressure is the referencing of choice in the continued work. The pegging methodology is though changed to peg the cylinder pressure *mean* value in the range  $-185^\circ$  to  $-175^\circ$  ATDC to intake manifold pressure. In this way the influence of noise on the pegging process is kept at a minimum.

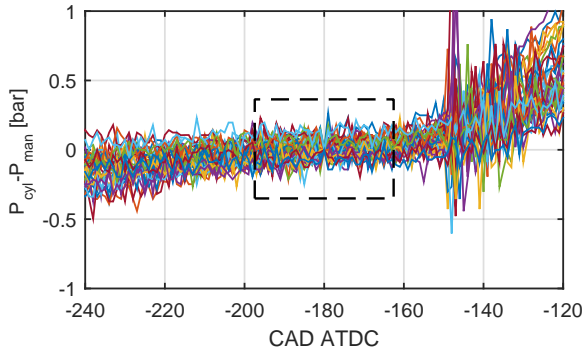


**Figure 5.2:** Pressure difference between MAP and in-cylinder pressure between  $-240^\circ$  and  $-120^\circ$  ATDC for all tested loads and speeds. No apparent speed or load dependent effects can be witnessed. At approximately  $-150^\circ$  ATDC the IVC is clearly seen as standing waves in the pressure signal.

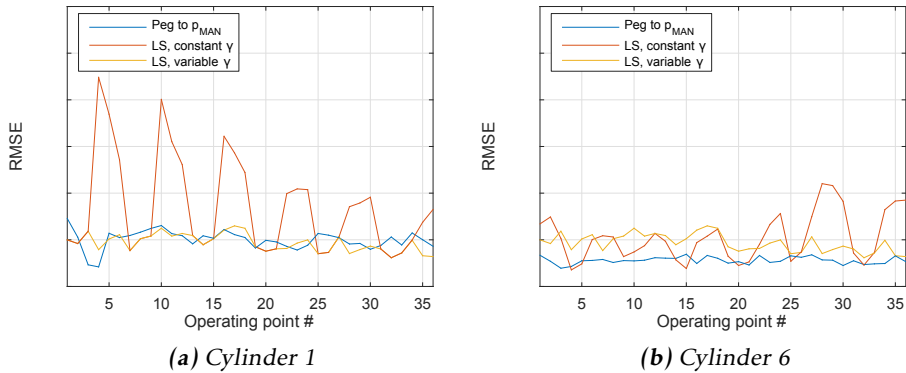


**Figure 5.3:** Absolute pressure reference by using manifold pressure and a polytropic model. All 36 operating points denoted as in Fig. 3.2. Cylinder 6 has better performance than cylinder 1 when using a polytropic model. However manifold pressure referencing show more stable performance. The sawtooth shape, especially on cylinder 1, is mitigated by adjusting  $\gamma$ .

## 5.4 Pressure sensor gain error

An objective is to detect and adjust gain errors on the pressure signal, see Section 4.1.3. In theory, this is not that difficult to solve. In practice however there have been major issues. The measured pressure was considered as having correct gain, thereby the algorithm should return a gain value of roughly one (1). Neither the isentropic compression with a polytropic model or the more advanced model based on gross heat-release gave satisfactory results. The advanced model did not result in any improvement. In Fig. 5.4 it can be seen that both models underestimate the measured pressure. Main causes for this was believed to depend on either the specific heat ratio,  $\gamma$ , compression ratio,  $r_c$ , or CAD phasing errors affecting the sampling of the pressure. Investigations showed that adding  $b-c$  to  $r_c$  give a more correct pressure at the end of the range. This enormous increase is of course unrealistic. Similarly, changing  $\gamma$  to a constant value of  $d$  seems to give more accurate values at the end. Though none of these "fixes" can give correct pressure between -90 to -30 CAD where the measured pressure is always higher.

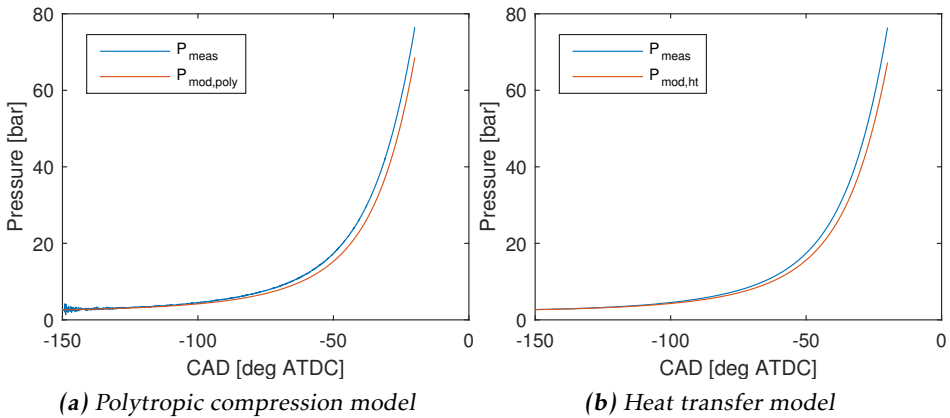


**Figure 5.4:** Two pressure models during compression are shown. Neither model is capable of describing the measured pressure. The cause is unknown and must be further investigated. Gain error compensation is therefore not possible in its current state.

The true cause for this effect has not been identified. Because of this, no compensation could be done to decrease gain error sensitivity.

To investigate the effect from an uncompensated error, a gain error was applied. As can be seen in Fig. 5.5, some effect is seen on both CA<sub>x</sub> and IMEP. IMEP show a deviation from nominal values for all operating points and fuels which is equal to the gain error. Gross heat-release is apparently more sensitive to gain errors compared to net heat-release. A possible explanation is that the heat transfer is affected by an erroneous pressure, thereby the error enters the calculation in two inputs instead of one which is the case for the net heat-release model.

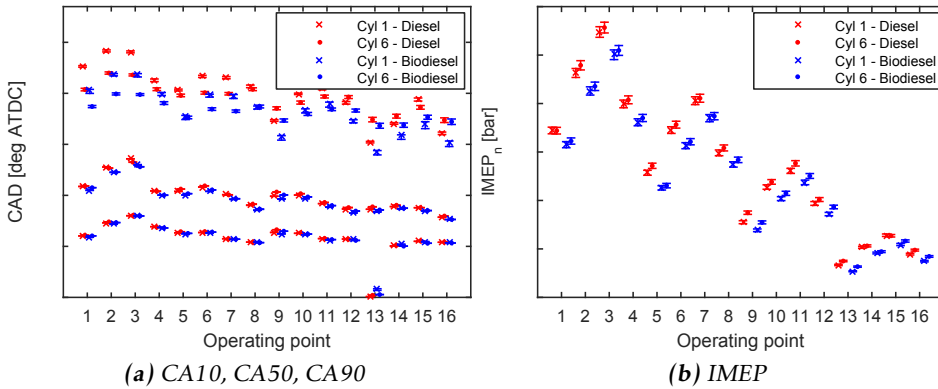


**Figure 5.5:** CAx and IMEP for cylinder 1 and 6 and diesel and biodiesel with a pressure sensor gain error. No noticeable effect can be seen on CAx while IMEP show some effect.

## 5.5 Specific heat ratio

A comparison was made between the selected models of  $\gamma$  as suggested in Section 4.2.2 to see how the model affects the heat-release. To quantify the effect CAx and total heat is the parameters of choice with deviations measured from  $\gamma_{NASA}$  with nominal values. Since ignition delay is calculated directly from pressure  $\gamma$  has no effect on that estimation (see Section 4.4.3), hence it is not included here. Results are summarised in Fig. 5.6.

A constant  $\gamma = e$  consistently estimates a higher total amount of heat, with largest deviation at 75% and 50% load combined with 1200 RPM and 800 RPM.  $\gamma_{lin}$  is estimating a higher amount of heat released at 50% to 100% load and a lower amount at 25% load. The largest deviation is seen at 100% load. This behaviour is consistent for both net and gross heat-release.

As can be clearly seen the choice of  $\gamma$  has a substantial impact on the heat-release, especially during later parts of combustion (CA50 and onwards). Selecting a constant  $\gamma$  will result in varying levels of errors depending on load and speed. At least a function of temperature should be used to minimise the CAx deviation. If CA50, CA90 and total amount of heat is important then careful consideration on model type should be made since  $\gamma$  has a large impact, in terms of absolute error, on these parameters.

During the rest of the tolerance analysis  $\gamma_{NASA}$  has been used in the heat-release calculations since it takes  $\lambda$  into consideration.

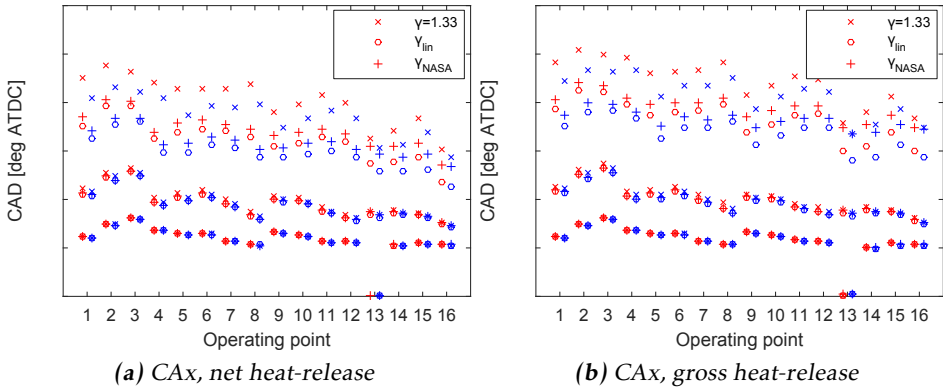


**Figure 5.6:** CAx for the net and gross heat-release. For CA10 and CA50 deviations are within  $1^\circ$  between all three variants while substantial impact can be seen at CA90, especially with a constant  $\gamma$ . The data plotted is for cylinder 6 for diesel (red) and biodiesel (blue). No difference could be observed for cylinder 1.

## 5.6 Heat-release models

To see how large difference in shape there is between net and gross heat-release, CA10, CA50 and CA90 were compared for nominal values with  $\gamma_{NASA}$ . Also the total amount of heat released in combustion and estimated amount of fuel injected are shown.

In Fig. 5.7 gross and net heat-release for both cylinders are shown. The most significant deviations are seen late in the combustion at CA90. An increasing absolute deviation can be seen across the combustion duration. It can be seen that deviations between cylinder 1 and 6 is approximately half of the deviations going from net to gross heat-release. The somewhat high cylinder-to-cylinder deviation is interesting to note. The total heat released noticeably deviates between cylinders. Looking at results at each operating point showed that deviations are low at high loads while they substantially increase at 50% load and lower, see Fig. 5.8. A possible explanation is torsion since cylinder 6 is closest to the crank angle sensor while cylinder 1 is furthest away. In an HDV torsion can be substantial at values above  $1^\circ$  on the far end of the crankshaft relative to the crank angle sensor. Directly comparing measured pressure show no large deviations when the difference in  $Q_{tot}$  is high.

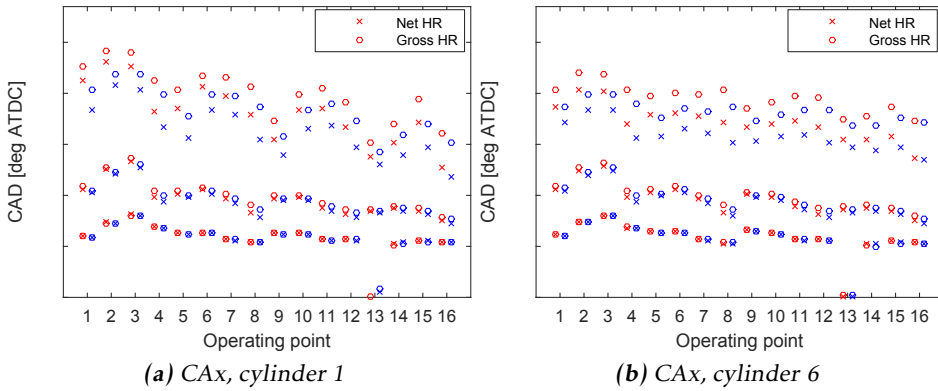


**Figure 5.7:** CAX comparison of the net and gross heat-release for (a) cylinder 1 and (b) cylinder 6. Red markers belong to standard diesel and blue markers belong to biodiesel.

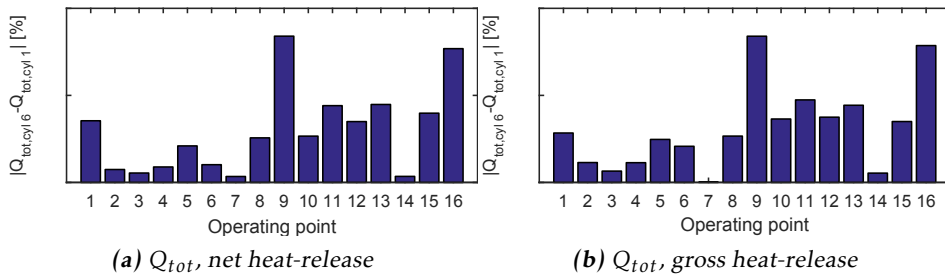


**Figure 5.8:**  $Q_{tot}$  deviation between cylinder 1 and 6 increases with lower loads. Data is only shown for standard diesel since biodiesel show the same behaviour.

### 5.6.1 Woschni heat transfer parameters

In the Woschni heat transfer model there exist several design parameters that depends on the engine being tested. In this work, the standard values given by Woschni has been used. To see how these parameters effect the results, a sensitivity analysis has been performed. The parameters  $C_1$ ,  $C_2$  has been changed from nominal Woschni values and  $T_w$  has been changed from a nominal value of 450 K. None of these injected errors gave a significant change in CAX or  $Q_{tot}$  values. CA90 is the most affected parameter but the change is low. It can be concluded that including the heat transfer model has a much larger impact on the heat-release than the exact determination of the correct parameters.

## 5.7 Crank angle phasing

As stated earlier TDC determination is complicated by the fact that pressure maximum does not coincide with TDC. The implemented algorithm tries to estimate the true position by positioning the motored cylinder pressure relative to the volume trace. In Fig. 5.9 estimations are shown for average pressure data with and without injected errors. Tests showed that there was no noticeable difference between estimating every cycle and average the results versus estimating directly on average pressure. Cylinder 1 shows significant dependence on speed while cylinder 6 gives stable estimations. Cylinder 1 is furthest away from the crank angle encoder which make it susceptible to torsion. Unfortunately the correct-

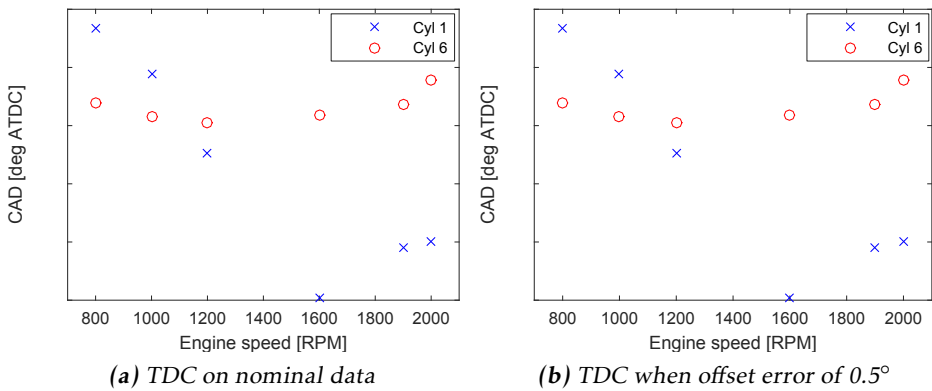


**Figure 5.9:** In (a) TDC estimation is made on nominal data. Cylinder 1 show speed dependent bias in estimations while cylinder 6 give stable results. In (b) an error is injected, effectively pushing  $p_{max}$  earlier than TDC. The offset is found and corrected in both cylinders, but with equal estimation bias.

ness of these estimations has not been possible to verify since the test equipment did not have any TDC sensor equipped. Results are consistent though which can be a small indicator that the estimation for cylinder 6 are somewhat correct. Torsional effects are minimised by mounting the pressure sensor on the cylinder closest to the crank angle encoder. However, to further evaluate the estimation quality, new measurements should be made combined with a TDC sensor.

Sensitivity to phasing errors is shown in Fig. 5.10 for CA<sub>x</sub> and IMEP. IMEP is significantly affected by a phasing error. CA<sub>90</sub> and  $Q_{tot}$  show high sensitivity while CA<sub>10</sub> and CA<sub>50</sub> show moderate changes. It can be concluded that phasing between pressure and volume is very important for accurate heat-release analysis. This fact stress the importance of the work by Rosvall [44], who investigate the problem of precise crank angle sampling by utilising a crankshaft torsion model.

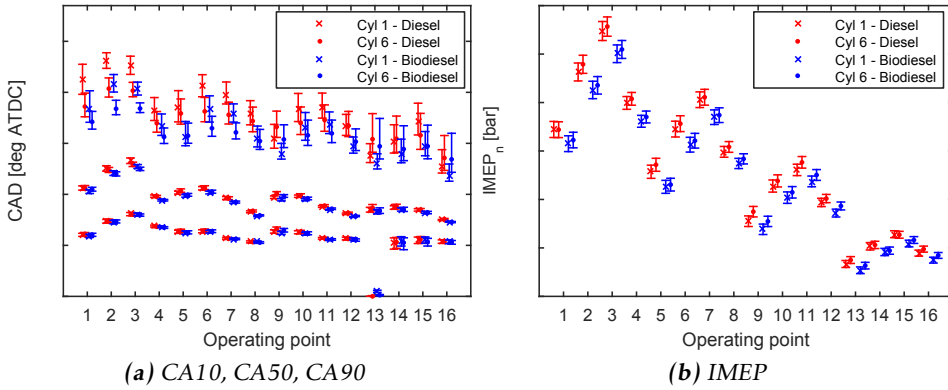


**Figure 5.10:** Nominal values and intervals for a crank phasing offset. It is moderately affecting the estimation of CA10 and CA50 while it has a major impact on CA90. An advanced offset gives advances CAx while a retarded offset delays CAx. Biodiesel advances CAx compared to diesel. In (b), IMEP is overestimated by an advanced offset while the opposite is true for a delayed offset. Biodiesel give considerably lower IMEP.

## 5.8 Compression ratio

A goal has been to estimate the compression ratio in an engine to adapt the ratio. The results have however been a let down with a large deviation from the nominal value. This is of course not good enough. It has been concluded that the model is probably too simple, and a future model has to take losses into account. A recommendation is to extend the gross heat-release implemented in this paper with a crevice model and perform an optimisation similar to Klein et al. [43]. Due to these results no compensation for compression ratio errors has been possible.

However, the sensitivity to compression ratio has been tested by adjusting the nominal value. As can be seen in Fig. 5.11, CAx is moderately affected and IMEP is unaffected, i.e.  $IMEP_n^{\Delta r_c} = IMEP_n^{nom}$ . Operating point 13 is "jumping" due to the error shifting the pilot injection just below 10% of total fuel amount, thereby CA10 detection happens at the ignition of the main injection 10° later.

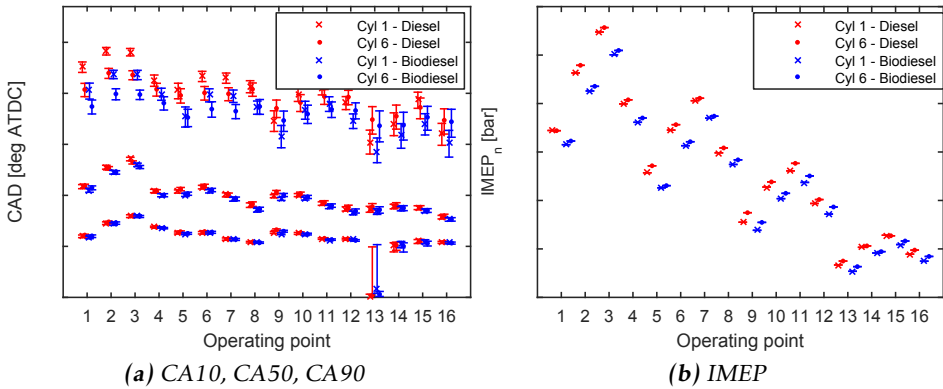


**Figure 5.11:** Nominal values and intervals for a compression ratio offset. An increased/decreased compression ratio retards/advances CA<sub>x</sub>, increasing with combustion duration. IMEP is not affected. Operating point 13 is not an outlier; the large deviation is caused by the pilot injection. An error pushes the pilot injection just below 10% of total fuel amount. The algorithm detects 10% when the main injection ignites.

## 5.9 Intake manifold sensor errors

External sensors needed in the implementation is boost temperature and boost pressure. These sensors are usually very accurate in their small measurement intervals. A typical boost temperature sensor has a total accuracy of  $\pm 2$  K. Such a small error showed no impact on any combustion parameters. Boost pressure is also very accurate with a total error of approximately  $\pm 0.05$  bar. Considering that the two high-accuracy in-cylinder pressure sensors used has a noise at IVC up to 0.3 bar, that inaccuracy is negligible.

## 5.10 Trapped mass error

Calculation of trapped mass is not entirely trivial considering the inaccuracies connected to IVC measurements: the valve takes time to close, residual gases remain in the cylinder, typically there is a pressure drop over the valve and compression ratio can be erroneous. Mass error is not significantly affecting CA<sub>x</sub> compared to other errors. It indirectly effects the heat-release by changing charge temperature which is input to the  $\gamma$ -model. Apparently the change in temperature is not changing  $\gamma$  by such an amount that it affects the heat-release in any significant way. Of course CA<sub>90</sub> shows increased deviation since it consistently is the most sensitive parameter to changes in inputs. Gross heat-release also shows some effect on total amount of heat released.

## 5.11 Effect of fuel type

Throughout the results section standard diesel (S10) and biodiesel (B100, 100% FAME) has been lumped together into a combined RMSE and maximum deviation. The reason for this is that investigations showed that the error sensitivity is typically not dependent on fuel type, only nominal values show significant changes. In this section, a direct comparison is made between the two tested fuels for nominal data.

Fig. 5.12 show how IMEP changes between fuels. IMEP is typically lower when using biodiesel. Operating point 5 and 13 show significantly larger differences than neighbouring operating points. The common denominator is a speed of 2000 RPM.

It can also be concluded from Fig. 5.7 that biodiesel advances all CAX. Biodiesel also contains less energy which is consistent with fuel data stating that S10 has a heating value of 42.93 MJ/kg while B100 has a value of 38 MJ/kg. This knowledge can be used to detect a change of fuel type by comparing CAX and  $Q_{tot}$  before and after refuelling.

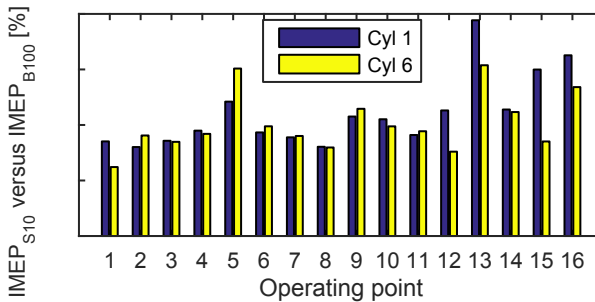


**Figure 5.12:** Effect on IMEP by changing to biofuel. A decrease can be expected in most operating points. Changes between cylinders increase at lower loads.

## 5.12 Validation of parametrisation model

To validate the closeness of fit between the triple Vibe model and the heat-release calculated from the measured pressure trace, a reconstructed pressure trace was created by inverting Eq. (4.20) or (4.21) depending on if the parametrisation is made on net or gross heat-release.

$$\frac{dp}{d\theta} = \frac{1}{V} \left( (\gamma - 1) \frac{dQ_{gross}}{d\theta} - (\gamma - 1) \frac{dQ_{ht}}{d\theta} - \gamma p \frac{dV}{d\theta} \right) \quad (5.1)$$

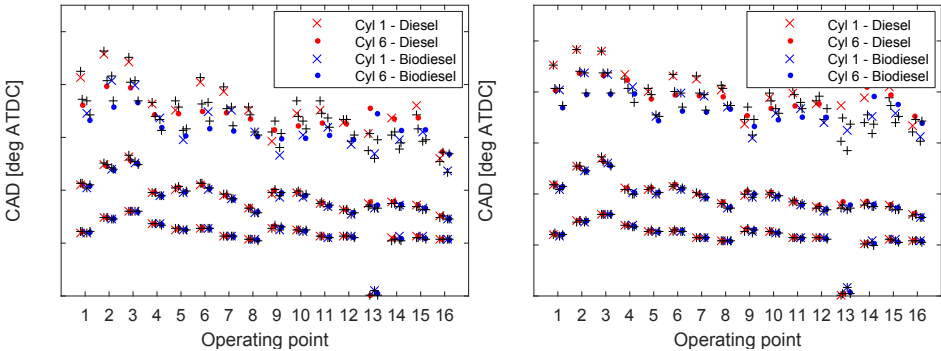
The differential equation was solved numerically with an Euler forward scheme,

$$p(k+1) = p(k) + \theta_{res} \frac{dp(k)}{d\theta} \quad (5.2)$$

where  $\theta_{res}$  is the step length.

To get a fully reconstructed pressure the starting pressure must be given in the Euler scheme. Two approaches are possible. Since the cylinder pressure is available it is best to save the cylinder pressure at SOI as an additional parameter, and run the reconstruction from there if only  $p_{max}$  and combustion parameters are of interest. Another approach is to model the compression stroke beginning at IVC. But as shown earlier, it is not as straightforward as it seems. When trying this approach large errors were common resulting in errors on  $p_{max}$  by equal magnitude.

In Fig. 5.13-5.14 results with the first approach is shown with good agreement to measured heat-release. Most problematic operating point to capture is low load with high speed (point number 13 and 14) where CA90 deviates significantly compared to other operating points. The chosen parametrisation is capable of accurately describing net and gross heat-release with standard diesel and biodiesel during most conditions.



(a) Net heat-release; CA10, CA50, CA90      (b) Gross heat-release; CA10, CA50, CA90

**Figure 5.13:** Nominal values for CAx calculated directly from measured pressure versus CAx calculated from parametrised heat-release. In (a) the parametrisation is done on the net heat-release and in (b) it is done on the gross heat-release. The black '+' is the reference value while 'x' and 'o' are the values estimated from the parametrised model.

To exemplify how dependent  $p_{max}$  is on correct starting pressure an offset is introduced, see Fig. 5.15. The error on  $p_{max}$  is generally of the same magnitude as the offset error in the reconstructed pressure.

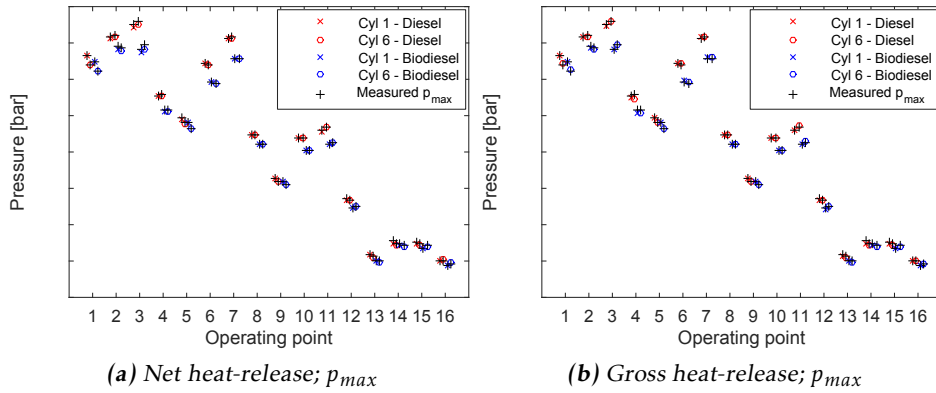


**Figure 5.14:** Maximum pressure from reconstructed pressure versus measured pressure. The parametrisation works equally well for net and gross heat-release regarding  $p_{max}$ .

It can be concluded that the chosen parametrisation works satisfactory and with high accuracy. More problematic areas are low loads where the combustion is erratic. Finally it must be stressed that the errors tested in previous sections will of course have a direct impact on the parametrisation, why it is important that errors are minimised in the stage of measurement.

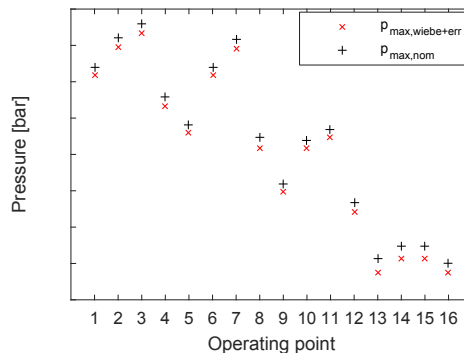


**Figure 5.15:** Maximum pressure from reconstructed pressure versus measured pressure. An offset on the reconstructed pressure is typically resulting in an equal offset on  $p_{max}$ .

# 6

---

## Conclusions

A thermodynamic analysis of the combustion in the cylinder has been implemented. From this it is possible to estimate multiple combustion parameters to be used in closed-loop combustion control. The implementation considers signal processing on the sensor inputs, estimations of TDC and compression ratio, choice of heat-release model and sub-models (for example specific heat ratio), and a thorough sensitivity analysis trying to identify the effect of fuel, mechanical tolerances and model parameters.

In the first part an adaptive filtering approach was implemented. However, the cutoff frequency was consistently set too high resulting in a very noisy pressure derivative, and subsequently a noisy heat-release on the verge of being useless for combustion parameter estimations. A Butterworth filter was used as replacement. For real-time filtering a Savitzky-Golay filter is recommended. To compensate for pressure drift, it is recommended to peg the pressure to intake manifold pressure at IBDC. A mean value over 10 CAD is used to minimise pegging error caused by noisy signals. Pegging by polytropic models is very sensitive even to small amounts of noise. If a polytropic model is used, a least-squares approach is recommended with at least 10 evenly spread points during the compression stroke. Gain error compensation has not been solved and the cause of the observed errors are still unknown and must be further investigated.

The second part, compression ratio and TDC estimation, has shown mixed results. Compression ratio is very difficult to estimate accurately. The selected model is too simple and does not take losses into account. Literature states that good estimations might be possible with a heat-release model with heat transfer and crevice effects, but the estimates are increasingly biased with higher compression ratios [43]. TDC determination has been difficult to verify without TDC sen-

sensor measurements. Estimations are stable on the cylinder closest to the flywheel where torsion effects are at a minimum, but the estimation bias is affected by the selection of CAD interval. Also, phasing errors from torsion and mechanical tolerances from CAD sensor to cylinder is a big concern. Phasing error is shown to be the single most affecting parameter after specific heat ratio, stressing the importance of minimising this sum of errors.

The final part, heat-release analysis, has been the most successful part. It is possible to estimate CA10, CA50, CA90, ignition delay, amount of fuel injected and engine efficiency. Directly from measured pressure the indicated torque, IMEP, SOC and  $p_{max}$  can be estimated. It has been found that implementing a heat transfer model has a significant impact on CAx. Very large differences are seen in late combustion where most of the heat transfer occurs. Following heat transfer the estimations are most sensitive to specific heat ratio and crank angle phasing. Gross heat-release has a higher sensitivity to pressure sensor gain error than net heat-release. As a final step, a heat-release parametrisation based on three Vibe functions has been made with good results on CAx and  $p_{max}$ . It is however dependent on good reconstruction of the compression pressure to give accurate results.

---

## Bibliography

- [1] Audi. Audi 3.0-liter V6 TDI with clean diesel system, 2009. URL [http://vwts.ru/engine/cata/ppps\\_941803\\_31\\_tdi\\_cata\\_w\\_clean\\_diesel\\_system\\_eng.pdf](http://vwts.ru/engine/cata/ppps_941803_31_tdi_cata_w_clean_diesel_system_eng.pdf). Cited on page 1.
- [2] BorgWarner Ludwigsburg GmbH. Borgwarner equips new generation of diesel engines from volkswagen with pressure sensor glow plugs, 2014. URL <http://www.beru.com/bw/borgwarner-equips-new-generation-of-diesel-engines-from-volkswagen-with-pressure-sensor-glow-plugs>. [Online; Accessed 18 February 2015]. Cited on pages 1 and 14.
- [3] C. A. Amann. Cylinder-pressure measurement and its use in engine research. *SAE Technical Papers*, Jan 1985. Cited on pages 3, 30, 36, and 37.
- [4] J. A. Gatowski, E. N. Balles, K. M. Chun, F. E. Nelson, J. A. Ekchian, and John B. Heywood. Heat release analysis of engine pressure data. In *SAE Technical Paper*. SAE International, 10 1984. Cited on pages 3 and 33.
- [5] John B. Heywood. *Internal Combustion Engine Fundamentals*. New York : McGraw-Hill, cop. 1988, 1988. ISBN 007028637X; 0071004998. Cited on pages 3, 8, 10, and 31.
- [6] M. F. J. Brunt and K. C. Platts. Calculation of heat release in direct injection diesel engines. *SAE Technical Papers*, Jan 1999. Cited on page 3.
- [7] Dimitrios T. Hountalas, Dimitrios A. Kouremenos, and Scott B. Fiveland. Some considerations on the estimation of the heat release of DI diesel engines using modelling techniques, Mar 2004. Cited on page 3.
- [8] Michael F. J. Brunt and Andrew L. Emtage. Evaluation of burn rate routines and analysis errors. *SAE Technical Papers*, Jan 1997. Cited on page 3.
- [9] M. Klein and L. Eriksson. A specific heat ratio model for single-zone heat release models. *SAE Technical Papers*, (2004), Jan 2004. Cited on page 3.
- [10] Michael F. J. Brunt, Harjit Rai, and Andrew L. Emtage. The calculation

- of heat release energy from engine cylinder pressure data, 1998. Cited on pages 3 and 31.
- [11] G. Woschni. A universally applicable equation for the instantaneous heat transfer coefficient in the internal combustion engine. *SAE Technical Papers*, Jan 1967. Cited on pages 4 and 31.
- [12] A. Antonopoulos and D. Hountalas. Identification and correction of the error induced by the sampling method used to monitor cylinder pressure of reciprocating internal combustion engines. *SAE Technical Papers*, / 01 / 01 / 2012. Cited on page 4.
- [13] F. Payri, J. M. Lujan, J. Martin, and A. Abbad. Digital signal processing of in-cylinder pressure for combustion diagnosis of internal combustion engines. *Mechanical Systems and Signal Processing*, 24(6):1767–1784, Aug 2010. Cited on page 4.
- [14] Emiliano Pipitone and Alberto Beccari. Determination of TDC in internal combustion engines by a newly developed thermodynamic approach. *Applied Thermal Engineering*, 30:1914–1926, 2010. Cited on pages 4 and 29.
- [15] Marek J. Stas. Thermodynamic determination of TDC in piston combustion engines. *SAE Technical Papers*, 1996. Cited on page 4.
- [16] Y. Nilsson and L. Eriksson. Determining TDC position using symmetry and other methods. *SAE Technical Papers*, (2004), Jan 2004. Cited on pages 4 and 29.
- [17] Richard S. Davis and Gary J. Patterson. Cylinder pressure data quality checks and procedures to maximize data accuracy. In *SAE Technical Paper*. SAE International, 04 2006. Cited on page 4.
- [18] Kangyoon Lee, Maru Yoon, and Myoungho Sunwoo. A study on pegging methods for noisy cylinder pressure signal. *Control Engineering Practice*, 16(8):922–929, 2008. ISSN 0967-0661. Cited on pages 4 and 14.
- [19] Andrew L. Randolph. Methods of processing cylinder-pressure transducer signals to maximize data accuracy. In *SAE Technical Paper*. SAE International, 02 1990. Cited on pages 4 and 14.
- [20] U. Asad and M. Zheng. Real-time heat release analysis for model-based control of diesel combustion. *SAE Technical Papers*, (2008), / 01 / 01 / 2008. Cited on page 4.
- [21] Usman Asad and Ming Zheng. Fast heat release characterization of a diesel engine, 2008. Not cited.
- [22] Stephen J. Citron, John E. O’Higgins, and Lillian Y. Chen. Cylinder by cylinder engine pressure and pressure torque waveform determination utilizing speed fluctuations, 1989. Cited on page 4.

- [23] C. J. Polonowski, V. K. Mathur, J. D. Naber, and J. R. Blough. Accelerometer based sensing of combustion in a high speed HPCR diesel engine. *SAE Technical Papers*, (2007), Jan 2007. Cited on page 4.
- [24] Ingemar Andersson and Lars Eriksson. Ion sensing for combustion stability control of a spark ignited direct injected engine, 2000. Cited on page 4.
- [25] M. Glavmo, P. Spadafora, and R. Bosch. Closed loop start of combustion control utilizing ionization sensing in a diesel engine. *SAE Technical Papers*, Mar 1999. Cited on page 4.
- [26] M. Thor, B. Egardt, T. McKelvey, and I. Andersson. Parameterized diesel engine combustion modeling for torque based combustion property estimation. *SAE Technical Papers*, Jan 2012. Cited on page 4.
- [27] John E. Dec. A conceptual model of DI diesel combustion based on laser-sheet imaging\*. In *SAE Technical Paper*. SAE International, 02 1997. Cited on page 8.
- [28] Lars Eriksson and Lars Nielsen. *Modeling and control of engines and drivelines*. Automotive series. Chichester, West Sussex, U.K. : John Wiley & Sons Ltd, 2014, 2014. ISBN 9781118536193. Cited on pages 11, 12, 13, and 35.
- [29] Tunestål, P. TDC offset estimation from motored cylinder pressure data based on heat release shaping. *Oil Gas Sci. Technol. – Rev. IFP Energies nouvelles*, 66(4):705–716, 2011. Cited on pages 13 and 29.
- [30] Markus Klein. *Single-Zone Cylinder Pressure Modeling and Estimation for Heat Release Analysis of SI Engines*. PhD thesis, Linköping University, Department of Electrical Engineering, The Institute of Technology, 2007. Cited on pages 13, 36, and 42.
- [31] Per Tunestål. *Estimation of the In-Cylinder Air/Fuel Ratio of an Internal Combustion Engine by the Use of Pressure Sensors*. 2001. Cited on pages 14 and 15.
- [32] G.P. Merker, C. Schwarz, and R. Teichmann. *Combustion Engines Development: Mixture Formation, Combustion, Emissions and Simulation*. Springer Berlin Heidelberg, 2011. ISBN 9783642140945. Cited on page 14.
- [33] Hans Houben, Bernd Last, and Frank Pechhold. Glow plug with integrated pressure sensor: A key component for closed-loop-combustion control, 2007. URL [http://www.beru.com/download/produkte/fachvortrag\\_psg\\_en.pdf](http://www.beru.com/download/produkte/fachvortrag_psg_en.pdf). [Online; Accessed 28 February 2015]. Cited on page 14.
- [34] M. T. Wlodarczyk, T. Poorman, L. Xia, J. Arnold, and T. Coleman. In-cylinder fiber-optic pressure sensors for monitoring and control of diesel engines. In *SAE Technical Paper*. SAE International, 08 1998. Cited on page 14.

- [35] Fredrik Gustafsson, Lennart Ljung, and Mille Millnert. *Signalbehandling*. Lund : Studentlitteratur, 2nd edition, 2001. ISBN 914401709X ; 9789144017099. Cited on page 15.
- [36] F. Payri, P. Olmeda, C. Guardiola, and J. Martín. Adaptive determination of cut-off frequencies for filtering the in-cylinder pressure in diesel engines combustion analysis. *Applied Thermal Engineering*, 31(14–15):2869 – 2876, 2011. ISSN 1359-4311. Cited on page 26.
- [37] Michael F. J. Brunt and Andrew L. Emtage. Evaluation of IMEP routines and analysis errors. *SAE Technical Papers*, 1996. Cited on page 29.
- [38] P. Pinchon. Calage thermodynamique du point mort haut des moteurs a piston. *Revue de l'institut francais du petrole*, 39(1):93–111, Jan 1984. Cited on page 29.
- [39] Lars Eriksson. Requirements for and a systematic method for identifying heat-release model parameters. In *SAE Technical Paper*. SAE International, Feb 1998. Cited on pages 30 and 36.
- [40] Bonnie J. McBride, Michael J. Zehe, and Sanford Gordon. NASA Glenn coefficients for calculating thermodynamic properties of individual species. 2002. URL <http://www.grc.nasa.gov/WWW/CEAWeb/TP-2002-211556.pdf>. Cited on page 32.
- [41] Lars Eriksson. Chepp - a chemical equilibrium program package for matlab. *SAE Transactions, Journal of Fuels and Lubricants*, 2004-01-1460, 4(113): 730–741, 2005. Cited on page 33.
- [42] I.I. Vibe. *Brennverlauf und Kreisprozess von Verbrennungsmotoren*. VEB Verlag Technik, 1970. Cited on page 35.
- [43] Marcus Klein, Lars Eriksson, and Jan Åslund. Compression ratio estimation based on cylinder pressure data. *Control Engineering Practice*, 14:197–211, 2006. Cited on pages 36, 50, and 55.
- [44] Tobias Rosvall. Design of virtual sensor for crank angle degree based on torque estimation, 2015. Cited on page 49.



## Upphovsrätt

Detta dokument hålls tillgängligt på Internet — eller dess framtida ersättare — under 25 år från publiceringsdatum under förutsättning att inga extraordinära omständigheter uppstår.

Tillgång till dokumentet innebär tillstånd för var och en att läsa, ladda ner, skriva ut enstaka kopior för enskilt bruk och att använda det oförändrat för icke-kommersiell forskning och för undervisning. Överföring av upphovsrätten vid en senare tidpunkt kan inte upphäva detta tillstånd. All annan användning av dokumentet kräver upphovsmannens medgivande. För att garantera äktheten, säkerheten och tillgängligheten finns det lösningar av teknisk och administrativ art.

Upphovsmannens ideella rätt innefattar rätt att bli nämnd som upphovsman i den omfattning som god sed kräver vid användning av dokumentet på ovan beskrivna sätt samt skydd mot att dokumentet ändras eller presenteras i sådan form eller i sådant sammanhang som är kränkande för upphovsmannens litterära eller konstnärliga anseende eller egenart.

För ytterligare information om Linköping University Electronic Press se förlagets hemsida <http://www.ep.liu.se/>

## Copyright

The publishers will keep this document online on the Internet — or its possible replacement — for a period of 25 years from the date of publication barring exceptional circumstances.

The online availability of the document implies a permanent permission for anyone to read, to download, to print out single copies for his/her own use and to use it unchanged for any non-commercial research and educational purpose. Subsequent transfers of copyright cannot revoke this permission. All other uses of the document are conditional on the consent of the copyright owner. The publisher has taken technical and administrative measures to assure authenticity, security and accessibility.

According to intellectual property law the author has the right to be mentioned when his/her work is accessed as described above and to be protected against infringement.

For additional information about the Linköping University Electronic Press and its procedures for publication and for assurance of document integrity, please refer to its www home page: <http://www.ep.liu.se/>